Wave propagation in periodic nano structures through second strain gradient elasticity

Wave propagation in periodic nano structures through second strain gradient elasticity

Bo Yang[a,d,*], Michele Bacciocchi[b], Nicholas Fantuzzi[a], Raimondo Luciano[c], Francesco Fabbrocino[d,**]

[a]*Department of Civil, Chemical, Environmental and Materials Engineering, University of Bologna, Viale del Risorgimento 2, 40136 Bologna, Italy*
[b]*Department of Economics, Sciences and Law, University of San Marino, Contrada Omerelli 20, 47890 San Marino, San Marino*
[c]*Department of Engineering, Parthenope University, Centro Direzionale ISOLA C4, 80133 Napoli, Italy*
[d]*Department of Engineering, Telematic University Pegaso, Centro Direzionale ISOLA F2, 80143 Napoli, Italy*

Abstract

The study of wave propagation in the periodic nano-waveguides is of importance to advance the development of energy and wave controlling systems. In this paper, firstly, the element discretization of nano structures is introduced based on the second strain gradient theory. The displacement field is determined through the utilization of six quintic Hermite polynomial interpolating functions. By applying Hamilton's principle, the weak form, which incorporates the element matrices, is determined and the global dynamic stiffness matrix of a unit cell is assembled. Then, the wave finite element method, based on the inverse form, direct form and contour integral solution, is used to analyze the two-dimensional free wave propagation properties of complex nano structures by solving the eigenvalue problems. The interpretation of the frequency spectrum is confined to the irreducible first Brillouin zone, encompassing both the dispersion relation and band structure. Furthermore, the slowness surfaces and energy flow vector fields are discussed via the second strain gradient theory. The novel work, which utilizes the second strain gradient theory equipped with the wave finite element method to investigate two-dimensional complex nano structures, has revealed significant potential in elucidating the two-dimensional wave propagation characteristics of the complex nano-waveguides.

Keywords: Wave propagation; Dispersion relation; Band structures; Second strain gradient elasticity; Complex nano structures

1. Introduction

The waveguides ranging from resonators, valves and switches have advanced the technologies in a wide range of field, including information processing, molecular manipulation and sensing. The

*Corresponding author: boyang-chn@hotmail.com (Bo Yang)
**Corresponding author: francesco.fabbrocino@unipegaso.it (Francesco Fabbrocino)

investigation for the heterogeneous waveguides can improve the performance and development of the existing wave and energy controlling systems. Initially, studies based on the Classical Theory (CT) of elasticity concentrated on the field of solid-state physic in the macro-sized materials [1–3]. For instance, Fu et al.[4] devised a singular boundary technique for investigating wave propagation at low to moderate wavenumbers in macro-periodic systems. It has been confirmed that the proposed technique produces satisfactory results and, as the number of boundary nodes increases, it converges to the exact solutions. Vescovini and Fantuzzi [5] studied the free vibrations for stiffened and unstiffened configurations. The result shows that the analytical evaluation of the Ritz integrals guarantees high efficiency. The experimental investigations into the dynamic properties of guided waves have recently garnered considerable attention. For instance, Fernando et al.[6] tested an impedance-graded multi-metallic system for a high velocity impact. It is demonstrated that the impedance-graded system has the capability of diminishing and reducing shock waves. Ravindran et al.[7] conducted an experimental study on a compaction wave within a low-density polymeric foam subjected to an intermediate-velocity projectile impact loading. The sound velocity determined analytically was in congruity with the precursor velocity observed experimentally.

Usually, in the macro-sized structures mentioned above, the local behavior of internal heterogeneity significantly impacts their dynamical properties; however, nano-materials exhibiting size effects demonstrate structural properties distinct from those at the macro-sized level [8, 9]. There are three main components of size effects. The first one is the large surface-to-volume ratio, which results in surface tension caused by energy associated with the particles on the structure's surface [10–12]. The second one is the micro-deformations: the structure's mechanical behavior is significantly influenced not only by the macro-deformations brought about by the macro-material, but also by the micro-deformations, including micro-rotation and micro-stretch, produced by the micro-material [13–15]. The last one is the non-local interactions: besides the local interactions, the non-local or long range interactions between different particles in the nano-sized structure can occur [16–18]. Due to the existence of the size effects, the propagation of waves in nano-materials can no longer be accurately estimated by the CT.

Interpreting the characteristics of nano-structures related to the size effects necessitates the utilization of non-classical continuum theories of elasticity, as illustrated in Fig.1, which can be categorized into the strain gradient family [19, 20], the micro-continuum theory [21, 22], the non-local elasticity theory [23, 24] and the surface elasticity theory [25, 26]. The strain gradient family consists of the couple stress theory [27–29], the First Strain Gradient (SG) theory [30, 31], the Second Strain Gradient (SSG) theory [32, 33] and the modified couple stress theory [34, 35]. In

couple stress theory, both the usual deformations and the gradient of the rotation vector are taken into consideration when calculating the strain energy. In modified couple stress theory, the assumption of symmetry of the couple stress tensor is used through the imposition of an equilibrium condition of couple moments. Mindlin put forward the SG theory, in which the strain and the first gradient of strain are employed to illustrate the elastic fields. However, the double stresses in the SG theory have singularities at the defect line [36]. Then, the SSG theory considering the double stresses and triple stresses was proposed to eliminate all the singularities of physical fields, such as the elastic bend-twist tensor and dislocation density tensor which are singular in the SG theory [37]. Most applications utilized SG theory instead of SSG elasticity primarily because SG theory is easier to handle mathematically, while the SSG theory is more complex. In the SSG theory, the energy density is a function of strain, the first derivative of strain, and the second derivative of strain. The SSG theory carries three distinct advantages: firstly, it is possible to remove all singularities which are still present in the SG theory; secondly, it allows for the confirmation of higher-order deformations caused by the higher-order scale lengths; and lastly, it explains the stiffness hardening from the long-range interactions. Since all the physical state quantities are smooth and non-singular through the SSG theory, utilizing a third strain gradient theory is unnecessary. On the other hand, the micro-continuum theory[38] consisting of the micro-polar theory, the micro-stretch theory and the micro-morphic theory is introduced here. The independent rotational scalar of the micro-material is taken into account in the micro-polar theory, while the independent stretching scalar of the micro-material is evaluated in the micro-stretch theory. The most general micro-morphic theory considers both the rotational and deformative behavior of the micro-material in the structure. In the non-local elasticity [39], the stress at a point is dependent upon the strains at all points of the body. A popularly employed model of surface elasticity[40] was developed by postulating a scalar coefficient.

The Lattice Spring Model (LSM) theory [41] has been demonstrated to be a valuable approach for elucidating the dynamic characteristics of nano-materials as well. The continuum governing equations of elasticity can be expressed through Fourier series transform according to the lattice governing equations. The LSM by the SSG relies upon the assumption that the force is reflective of a non local interaction between particles, introducing a relation with nearest, next nearest and next next nearest interactions, thus constituting a new type of elastic material with non-local characters. As presented in Fig.1, the detailed concept of each theory and the connections between different theories are elaborated. If the value of non-classical part in each theory is considered to be 0, the non-classical theory will return to the CT.

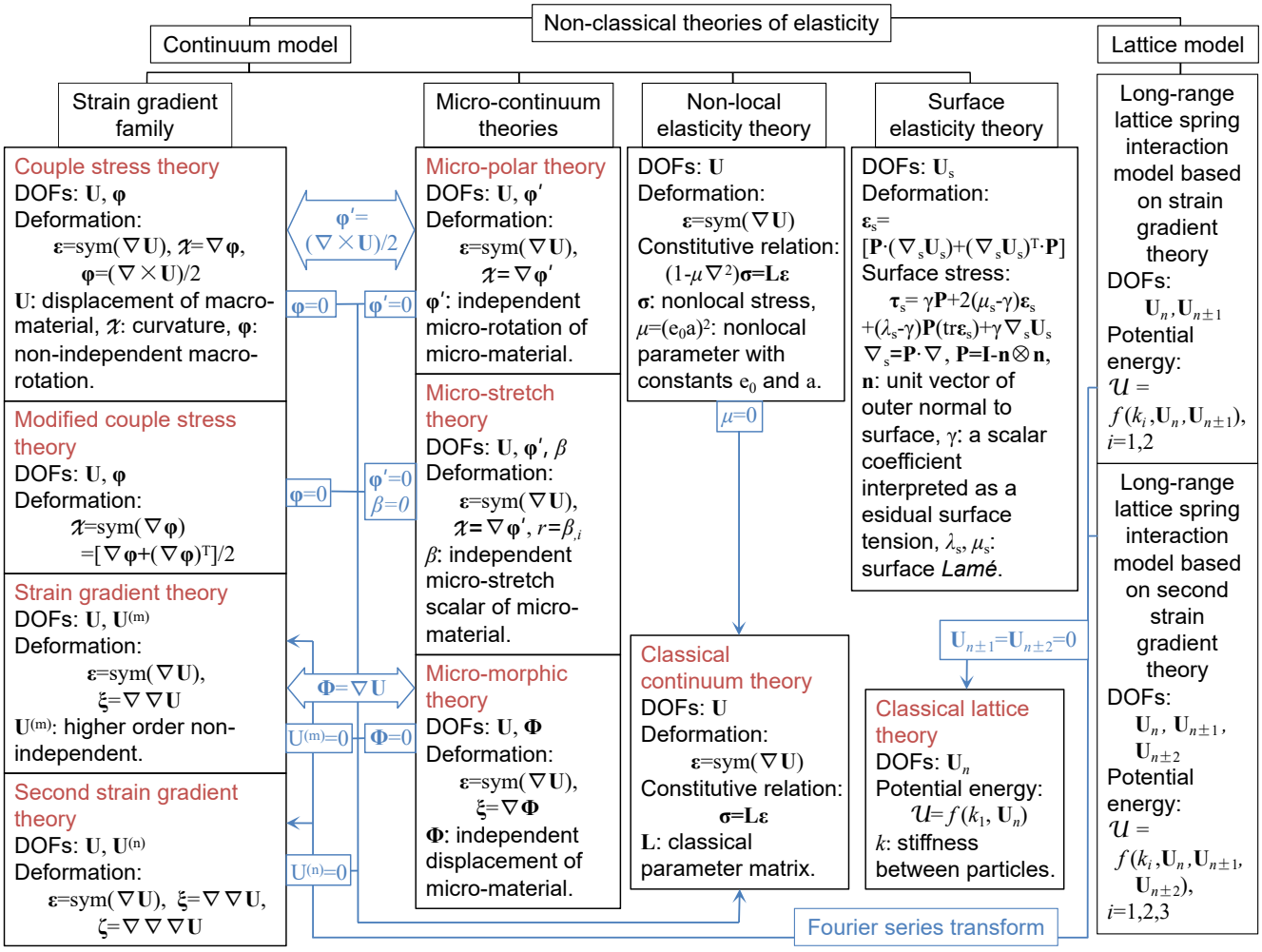

Fig. 1: State-of-the-art of non-classical theories of elasticity for nano-structures.

Recently, researchers have undertaken explorations of the properties of nano or micro-structures utilizing non-classical theories. For example, Bruno and Kachanov [42] discussed the potential of micromechanics in the formation of microstructures, including nonlinear stress–strain behavior and effective elastic properties. Bacciocchi et al. [43–45] developed a finite element method for the numerical investigation of static and dynamic problems of laminated plates, accounting for the nonlocal strain gradient effect. Tocci Monaco et al. [46] explored the flexural behavior of nanoplates in response to both sinusoidal and uniform loading through the semi-analytical strain gradient theory. The result shows a good agreement with the one from literature. Furthermore, Fu et al. [47] studied the dynamical properties of the isotropic materials through the analytical strain gradient elasticity theory and predicted the material length-scale parameters and the deflections in the nano materials. Tuna et al. [48, 49] investigated the 'explicit' and 'implicit' non-local continuum models through the micro-polar theory. It demonstrates that the proposed method is efficacious for depicting the mechanical behaviour of complex materials. Meanwhile, Fantuzzi et al.

[50] deduced the constitutive parameters of composite materials via a homogenization technique equipped with the micro-polar theory. Żur et al. [51–53] introduced a variational principle and studied the properties of ultra-small structures via the higher-order gradient elasticity.

On the other hand, a Wave Finite Element Method (WFEM) [54–57] has been proposed to investigate wave propagation in complex periodic structures, and can be progressed from traditional FE method to enable the modeling of multiple intricate structures. The WFEM is capable of reducing a periodic structure into a unit cell according to the periodic structure theory [58, 59], thereby reducing the computational effort involved. The dynamic properties can be elucidated through the spectral analysis of the unit cell [60]. Regarding the numerical simulation, a number of works about the wave propagation characteristics can be found. For instance, Xiao et al. [61] studied the flexural wave propagation in beams with periodically attached vibration absorbers. It shows that the presence of both resonance-type and Bragg-type band gaps is a result of the coexistence of local resonance and spatial periodicity. Wei et al. [62] demonstrated the wave properties by analyzing the acoustic tensors of extremal materials. Their finding reveals that the quantity of slowness surfaces can be determined based on the number of distinct characteristic force vectors originating from the hard modes on a given wave front plane. What is more, Zhang et al. [63] conducted calculations on group velocities to investigate how geometrical parameters impact directional frequency-dependent energy flows within structures. It indicates that in the auxetic chiral structure, the first mode of the elastic wave propagates exclusively along particular specified directions. Nguyen et al. [64] introduced a novel deep learning technique to study the wave propagation in media with multi-scale wave speed. The study demonstrates that the trained neural networks can effectively approximate the nonlinear relationship between wave propagation and wave speed.

In this paper, firstly, the 1D periodic structure technique used in the simple structures was extended to the heterogeneous 2D nano structures. As far as the authors are aware, the WFEM has never been exploited to investigate 2D wave propagation (e.g., slowness surfaces, band structure and energy flow) equipped with the SSG theory in complex 2D nano structures. Secondly, the exploration of dynamic properties for nano structures was enriched. Actually, there exist more complex waves such as higher-order waves in the realistic structures. The potential dynamic properties of complex nano structures cannot be obtained by studying the conventional waves (e.g., bending, tension and shearing) only. The exploration of multi-mode propagation is of great importance. Furthermore, the new insights on the stiffness hardening phenomena and size-dependent characteristics were given. These properties have significant impacts on the results but can not

be explained by the classical theories. Reflecting the size effects and stiffness hardening caused by higher-order parameters into the WFEM framework is a novel and valuable approach to study the dynamic properties of nano structures effectively. Lastly, the Contour Integral (CI) solution was combined with the SSG theory to solve the eigenvalue problem for the first time. The results match the ones from the traditional direct form solution well.

The primary objectives of this work are to confirm the element discretization of complex nano structures using the SSG theory and to analyze the free 2D wave propagation properties by solving the eigenvalue problems through the WFEM. The combination of the WFEM with the SSG theory is necessary in order to study the dynamic characteristics of complex periodic structures, and to investigate the size effects existing in nano-sized materials.

The structure of the article is as follows: Section 2 introduces the constitutive relations of the 3D nano-sized model via the SSG theory, and provides the weak form, comprising the element matrices. Section 3 presents the free 2D wave propagation characteristics, deduced from the eigenvalue problem solved via the WFEM. Section 4 explains the wave dispersion, slowness surfaces, band structure, and energy flow. Finally, some conclusions are outlined in Section 5.

2. Finite element discretization through the SSG theory

Within the SSG theory framework, this part introduces the constitutive relations of a 3D nano-structure. Subsequently, employing six quin-tic Hermite polynomial interpolating functions, the displacement vector is deduced. Finally, the weak formulation is interpreted through utilizing Hamilton's principle.

2.1. Constitutive relations

The strain energy density $\overline{\mathcal{U}}$ proposed by Mindlin [32] within the SSG theory framework is expressed below:

$$\begin{aligned}\overline{\mathcal{U}} =& \frac{1}{2}\lambda\varepsilon_{ii}\varepsilon_{jj} + \mu\varepsilon_{ij}\varepsilon_{ij} + a_1\xi_{ijj}\xi_{ikk} + a_2\xi_{iik}\xi_{kjj} + a_3\xi_{iik}\xi_{jjk} + a_4\xi_{ijk}\xi_{ijk} + a_5\xi_{ijk}\xi_{jki} + b_1\zeta_{iijj}\zeta_{kkll} \\ &+ b_2\zeta_{ijkk}\zeta_{ijll} + b_3\zeta_{iijk}\zeta_{jkll} + b_4\zeta_{iijk}\zeta_{llkj} + b_5\zeta_{iijk}\zeta_{lljk} + b_6\zeta_{ijkl}\zeta_{ijkl} + b_7\zeta_{ijkl}\zeta_{jkli} + c_1\varepsilon_{ii}\zeta_{jjkk} \\ &+ c_2\varepsilon_{ij}\zeta_{ijkk} + c_3\varepsilon_{ij}\zeta_{kkij},\end{aligned} \tag{1}$$

where $\boldsymbol{\varepsilon}$=$sym(\nabla\mathbf{U})$, $\boldsymbol{\xi}$=$\nabla\boldsymbol{\varepsilon}$, $\boldsymbol{\zeta}$=$\nabla\nabla\boldsymbol{\varepsilon}$, $\mathbf{U}$ indicates the displacement vector, ∇ is the gradient operator, λ and μ are related to the Young's modulus E, Poisson's ratio ν and shear modulus G

by the equations $\lambda = \nu E/(1+\nu)(1-2\nu)$ and $\mu = G = E/2(1+\nu)$. Additionally, a_i, b_i and c_i are the higher-order parameters, which can be determined through the inter-atom potential function approach [65]. $a_{i(i=1,\ldots,5)}$ are related to the first derivative of strain. $b_{i(i=1,\ldots,7)}$ are related to the second derivative of strain. $c_{i(i=1,\ldots,3)}$ are related to the part coupled by the strain and second derivative of strain. In this work, in order to make sure the structure macroscopically isotropic and use the SSG formulation reasonably, the size of the structure is defined much larger than that of a crystal unit in the structure.

The vector of the displacement field in the 3D Cartesian coordinate system (x, y, z) is expressed as:

$$\mathbf{U}(x,y,z,t) = \{u_1(x,y,z,t), u_2(x,y,z,t), u_3(x,y,z,t)\}^{\mathrm{T}}, \tag{2}$$

where u_1, u_2 and u_3 are the the displacements along the x, y and z direction, respectively. Superscript T indicates the transpose of matrix or vector.

The strain energy density addressed by the $\boldsymbol{\varepsilon}$, $\boldsymbol{\xi}$ and $\boldsymbol{\zeta}$ can be verified as:

$$\boldsymbol{\varepsilon} = \boldsymbol{\Psi}_1\mathbf{U},\ \boldsymbol{\xi} = \boldsymbol{\Psi}_2\mathbf{U},\ \boldsymbol{\zeta} = \boldsymbol{\Psi}_3\mathbf{U}, \tag{3}$$

where $\boldsymbol{\Psi}_1$, $\boldsymbol{\Psi}_2$ and $\boldsymbol{\Psi}_3$ are represented in Appendix A.

Then, based on the SSG theory, the constitutive relations of the 3D model can be established:

$$\boldsymbol{\tau}_1 = \mathbf{L}\boldsymbol{\varepsilon} + \mathbf{C}\boldsymbol{\zeta},\ \boldsymbol{\tau}_2 = \mathbf{A}\boldsymbol{\xi},\ \boldsymbol{\tau}_3 = \mathbf{B}\boldsymbol{\zeta} + \mathbf{C}^{\mathrm{T}}\boldsymbol{\varepsilon}, \tag{4}$$

where the expressions of $\mathbf{L}_{(6\times6)}$, $\mathbf{A}_{(18\times18)}$, $\mathbf{B}_{(30\times30)}$ and $\mathbf{C}_{(6\times30)}$ are addressed in Appendix B. Consequently, the strain energy density can be expressed in the matrix form through the SSG theory:

$$\overline{\mathcal{U}} = \frac{1}{2}\boldsymbol{\varepsilon}^{\mathrm{T}}\mathbf{L}\boldsymbol{\varepsilon} + \frac{1}{2}\boldsymbol{\xi}^{\mathrm{T}}\mathbf{A}\boldsymbol{\xi} + \frac{1}{2}\boldsymbol{\zeta}^{\mathrm{T}}\mathbf{B}\boldsymbol{\zeta} + \boldsymbol{\varepsilon}^{\mathrm{T}}\mathbf{C}\boldsymbol{\zeta}. \tag{5}$$

2.2. Element matrices

After obtaining the matrix form of the strain energy density, the weak form will be computed in this part. The node DOFs for the 1D and 3D Hermite elements are depicted in Fig.2.

A six-term polynomial function is employed to interpolate the scalar field U_1=$u_1(\overline{x}, t)$ inside a 1D element, which ensures the continuity between the 1D elements, as follows:

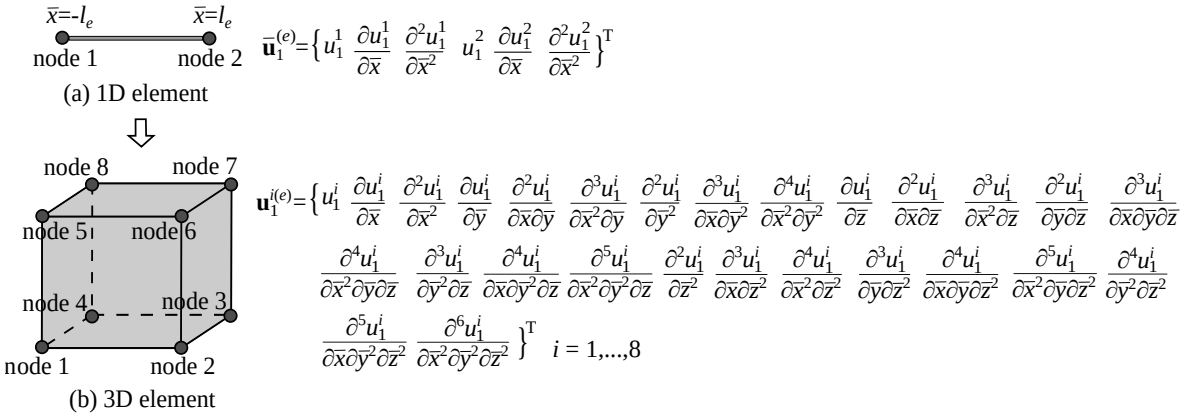

Fig. 2: Definition of the node numbers and nodal degree of freedoms (DOFs) for the one-dimensional and three-dimensional Hermite elements with C^2 continuity. $\overline{\mathbf{u}}_1^{(e)}$ is the DOFs vector for the 1D element. $\mathbf{u}_1^{i(e)}$ indicates the DOFs on the 3D element nodes. l_e is the half length of the 1D element. ($\overline{x}$, $\overline{y}$, $\overline{z}$) are the local Cartesian coordinate system.

$$\mathrm{U}_1 = \{1, \overline{x}, \overline{x}^2, \overline{x}^3, \overline{x}^4, \overline{x}^5\}\{\mathrm{s}_0, \mathrm{s}_1, \mathrm{s}_2, \mathrm{s}_3, \mathrm{s}_4, \mathrm{s}_5\}^{\mathrm{T}} = \mathbf{xs}. \tag{6}$$

As shown in Fig.2 (a), the $\overline{\mathbf{u}}_1^{(e)}$, named as the nodal displacement vector in a 1D element, can be evaluated as follows:

$$\overline{\mathbf{u}}_1^{(e)} = \{\mathbf{d}_1, \mathbf{d}_2, \mathbf{d}_3, \mathbf{d}_4, \mathbf{d}_5, \mathbf{d}_6\}^{\mathrm{T}}\mathbf{s} = \mathbf{ds}, \tag{7}$$

where $\mathbf{d}_1$=$\{1,\ -l_e,\ l_e^2,\ -l_e^3,\ l_e^4,\ -l_e^5\}$, $\mathbf{d}_2$=$\{0,\ 1,\ -2l_e,\ 3l_e^2,\ -4l_e^3,\ 5l_e^4\}$, $\mathbf{d}_3$=$\{0,\ 0,\ 2,\ -6l_e,\ 12l_e^2,\ -20l_e^3\}$, $\mathbf{d}_4$=$\{1,\ l_e,\ l_e^2,\ l_e^3,\ l_e^4,\ l_e^5\}$, $\mathbf{d}_5$=$\{0,\ 1,\ 2l_e,\ 3l_e^2,\ 4l_e^3,\ 5l_e^4\}$, $\mathbf{d}_6$=$\{0,\ 0,\ 2,\ 6l_e,\ 12l_e^2,\ 20l_e^3\}$. Then, by combining Eq.7 with Eq.6, the displacement vector can be expressed in terms of the six quintic Hermite polynomial interpolating functions and the nodal displacement vector, as follows:

$$\mathrm{U}_1 = \mathbf{xd}^{-1}\overline{\mathbf{u}}_1^{(e)} = \mathbf{S}(\overline{x})\overline{\mathbf{u}}_1^{(e)}, \tag{8}$$

in which the interpolating functions $\mathbf{S}(\overline{x})$ are expressed as:

$$\mathbf{S}(\overline{x}) = \left\{\mathrm{S}_1^0(\overline{x}), \mathrm{S}_1^1(\overline{x}), \mathrm{S}_1^2(\overline{x}), \mathrm{S}_2^0(\overline{x}), \mathrm{S}_2^1(\overline{x}), \mathrm{S}_2^2(\overline{x})\right\}, \tag{9}$$

where $\mathrm{S}_1^0(\overline{x})$, $\mathrm{S}_1^1(\overline{x})$, $\mathrm{S}_1^2(\overline{x})$, $\mathrm{S}_2^0(\overline{x})$, $\mathrm{S}_2^1(\overline{x})$ and $\mathrm{S}_2^2(\overline{x})$ are shown in Appendix C.

On the other hand, the interpolating functions in the $\overline{y}$ and $\overline{z}$ directions can be deduced as: $\mathbf{S}(\overline{y})|_{(\overline{y}=\overline{x})}$=$\{\mathrm{S}_1^0(\overline{y}),\mathrm{S}_1^1(\overline{y}),\mathrm{S}_1^2(\overline{y}),\mathrm{S}_2^0(\overline{y}),\mathrm{S}_2^1(\overline{y}),\mathrm{S}_2^2(\overline{y})\}$, $\mathbf{S}(\overline{z})|_{(\overline{z}=\overline{x})}$=$\{\mathrm{S}_1^0(\overline{z}),\mathrm{S}_1^1(\overline{z}),\mathrm{S}_1^2(\overline{z}),\mathrm{S}_2^0(\overline{z}),\mathrm{S}_2^1(\overline{z}),\mathrm{S}_2^2(\overline{z})\}$. Subsequently, the hexahedral element's interpolating functions, depicted in Fig. 2 (b), is established by extending a 1D element to a 3D element [66, 67]:

$$\mathbb{S}(\overline{x},\overline{y},\overline{z}) = \left\{\mathbf{S}_1(\overline{x},\overline{y},\overline{z})\otimes\mathbf{E}_1,\ \mathbf{S}_2(\overline{x},\overline{y},\overline{z})\otimes\mathbf{E}_2,\ \mathbf{S}_3(\overline{x},\overline{y},\overline{z})\otimes\mathbf{E}_3\right\}^{\mathrm{T}}, \tag{10}$$

in which the elements in the $\mathbf{S}_q(\overline{x},\overline{y},\overline{z})$ and $\mathbf{E}_q$ $(p=1,2,3)$ are expressed as follows:

$$\begin{aligned} &\mathrm{S}_q^{i(u,v,w)}(\overline{x},\overline{y},\overline{z}) = \mathrm{S}_j^u(\overline{x})\mathrm{S}_k^v(\overline{y})\mathrm{S}_l^w(\overline{z}),\\ &\mathbf{E}_q = \left\{\epsilon_{q1},\epsilon_{q2},\epsilon_{q3}\right\}, \end{aligned} \tag{11}$$

where $i=1,...,8$. $u,v,w=0,1,2$. $\mathrm{S}_q^{i(j,k,l)}(\overline{x},\overline{y},\overline{z})$ is connected with the DOFs $\partial^{u+v+w}u_1^i/(\partial\overline{x}^u\partial\overline{y}^v\partial\overline{z}^w)$ of node i in the hexahedron element. The notation $j,k,l=1,2$ signifies the node numbering within the respective 1D element, which can be established as either 1 or 2 depending on whether i is $-l_e$ or l_e, respectively. Furthermore, the symbol ϵ_{qr} is equal to 0 if $q\neq r$ and equal to 1 if $q=r$ for any value of r from the set $1,2,3$.

Within the 3D element, the displacement vector $\mathbf{U}(\overline{x},\overline{y},\overline{z})$ can be written as:

$$\mathbf{U}(\overline{x},\overline{y},\overline{z},t) = \mathbb{S}(\overline{x},\overline{y},\overline{z})\mathbf{u}^{(e)}(t), \tag{12}$$

where $\mathbb{S}(\overline{x},\overline{y},\overline{z})$ is the 3D interpolating functions, $\mathbf{u}^{(e)}=\{\mathbf{u}_1^{(e)\mathrm{T}},\mathbf{u}_2^{(e)\mathrm{T}},\mathbf{u}_3^{(e)\mathrm{T}}\}^{\mathrm{T}}$, $\mathbf{u}_p^{(e)\mathrm{T}}=\{\mathbf{u}_p^{1(e)\mathrm{T}},\mathbf{u}_p^{2(e)\mathrm{T}},\ ...,\ \mathbf{u}_p^{8(e)\mathrm{T}}\}^{\mathrm{T}}$ $(p=1,2,3)$. Subsequently, the potential energy $\mathcal{U}$ can be acquired through the integration of the strain energy density:

$$\mathcal{U} = \int_V \overline{\mathcal{U}}\mathrm{d}V = \frac{1}{2}\mathbf{u}^{(e)\mathrm{T}}\mathbf{K}^{(e)}\mathbf{u}^{(e)}. \tag{13}$$

On the other hand, the kinetic energy is expressed as [68]:

$$\mathcal{T} = \frac{1}{2}\rho\int_\Omega\left(\dot{\mathbf{U}}\cdot\dot{\mathbf{U}} + l_1^2\nabla\dot{\mathbf{U}}:\nabla\dot{\mathbf{U}} + l_2^4\nabla\nabla\dot{\mathbf{U}}\vdots\nabla\nabla\dot{\mathbf{U}}\right)\mathrm{d}\Omega, \tag{14}$$

in which the linear mass density, represented by ρ, and the higher-order length-scale parameters, denoted by l_1 and l_2, are used. In this work, the classical part of the kinetic energy related to the macro-inertia is considered only. The mass is composed of two parts which come from the macro-material related to the macro-inertia and the micro-material related to the micro-inertia respectively per unit volume in nano-structure [30]. The main influence of the mass on the mechanical properties comes from the macro-inertia. The effect of micro-inertia is prevalent at high frequencies, but its impact is secondary in comparison to the macro-inertia, and therefore, often neglected [69]. As a result:

$$\mathcal{T} = \frac{1}{2}\int_V \left(\frac{\partial \mathbf{U}}{\partial t}\right)^{\mathrm{T}} \rho \left(\frac{\partial \mathbf{U}}{\partial t}\right) \mathrm{d}V = \frac{1}{2}\left(\frac{\partial \mathbf{u}^{(e)}}{\partial t}\right)^{\mathrm{T}} \mathbf{M} \left(\frac{\partial \mathbf{u}^{(e)}}{\partial t}\right). \tag{15}$$

In the meantime, the external force's effect on the work done, represented by $\delta\mathcal{W}$, is expressed as follows:

$$\delta\mathcal{W} = \int_V \delta\mathbf{U}^{\mathrm{T}}\mathbf{f}_V \mathrm{d}V + \int_S \delta\mathbf{U}^{\mathrm{T}}\mathbf{f}_S \mathrm{d}S = \delta\mathbf{u}^{(\mathrm{e})\mathrm{T}}\mathbf{F}^{(e)}, \tag{16}$$

in which $\mathbf{f}_V$ indicates the volume force, $\mathbf{f}_S$ represents the face force. Finally, by introducing the Hamilton's principle:

$$\int_{t_1}^{t_2} (\delta\mathcal{W} - \delta\mathcal{U} + \delta\mathcal{T})\,\mathrm{d}t = \int_{t_1}^{t_2} \left[\delta\mathbf{u}^{(e)\mathrm{T}} \left(\mathbf{M}^{(e)}\frac{\partial^2 \mathbf{u}^{(e)}}{\partial t^2} + \mathbf{K}^{(e)}\mathbf{u}^{(\mathrm{e})} - \mathbf{F}^{(e)}\right)\right] \mathrm{d}t = 0, \tag{17}$$

the stiffness and mass matrices of the 3D element, along with the force vector, can be formulated as follows:

$$\begin{aligned}
\mathbf{K}^{(e)} &= \int_V \left(\mathbb{S}^{\mathrm{T}}\boldsymbol{\Psi}_1^{\mathrm{T}}\mathbf{L}\boldsymbol{\Psi}_1\mathbb{S} + \mathbb{S}^{\mathrm{T}}\boldsymbol{\Psi}_2^{\mathrm{T}}\mathbf{A}\boldsymbol{\Psi}_2\mathbb{S} + \mathbb{S}^{\mathrm{T}}\boldsymbol{\Psi}_3^{\mathrm{T}}\mathbf{B}\boldsymbol{\Psi}_3\mathbb{S} + 2\mathbb{S}^{\mathrm{T}}\boldsymbol{\Psi}_1^{\mathrm{T}}\mathbf{C}\boldsymbol{\Psi}_3\mathbb{S}\right)\mathrm{d}V, \\
\mathbf{M}^{(e)} &= \int_V \left(\mathbb{S}^{\mathrm{T}}\rho\mathbb{S}\right)\mathrm{d}V, \\
\mathbf{F}^{(e)} &= \int_V \left(\mathbb{S}^{\mathrm{T}}\mathbf{f}_V\right)\mathrm{d}V + \int_S \left(\mathbb{S}^{\mathrm{T}}\mathbf{f}_S\right)\mathrm{d}S.
\end{aligned} \tag{18}$$

3. Wave propagation within the WFEM framework

Upon procuring the matrices representing the 3D element matrices, the present section initiates by deducing the unit cell's dynamic equation. Subsequently, a 2D wave propagation analysis is performed by solving the eigenvalue problems under free and periodic boundary conditions.

The formulation of the dynamic equilibrium of a unit cell, as outlined by the WFEM, can be expressed as follows:

$$\mathbf{K}\mathbf{u}(t) + \mathbf{Q}\frac{\partial \mathbf{u}(t)}{\partial t} + \mathbf{M}\frac{\partial^2 \mathbf{u}(t)}{\partial t^2} = \mathbf{F}, \tag{19}$$

where the unit cell stiffness matrix, $\mathbf{K}$, and mass matrix, $\mathbf{M}$, are constructed through the assembly of element stiffness ($\mathbf{K}^{(e)}$) and mass ($\mathbf{M}^{(e)}$) matrices, respectively. The damping matrix, $\mathbf{Q}$, is represented by $\mathbf{Q} = \eta\mathbf{K}/\omega$ and takes into account the damping loss factor, η, which is caused by internal friction within the material. The nodal displacement vector is denoted by $\mathbf{u}$, and the force vector is represented by $\mathbf{F}$. Given harmonic $\mathbf{u}$ and $\mathbf{F}$, the dynamic stiffness matrix can be

represented in the frequency domain as $\mathbf{D} = \tilde{\mathbf{K}} - \omega^2\mathbf{M}$, where $\tilde{\mathbf{K}} = (1+\mathrm{i}\eta)\mathbf{K}$. By categorizing the DOFs into internal (I) and boundary (Bd) DOFs, Eq. 19 can be re-expressed. It is noteworthy to mention that the DOFs on internal nodes of a unit are not impacted by external loads as the coupling relations are restricted solely to their boundaries, as stated in [58]. So, $\mathbf{F}_\mathrm{I} = 0$, this yields:

$$\begin{bmatrix} \mathbf{D}_{\mathrm{BdBd}} & \mathbf{D}_{\mathrm{BdI}} \\ \mathbf{D}_{\mathrm{IBd}} & \mathbf{D}_{\mathrm{II}} \end{bmatrix} \begin{Bmatrix} \hat{\mathbf{u}}_{\mathrm{Bd}} \\ \hat{\mathbf{u}}_{\mathrm{I}} \end{Bmatrix} = \begin{Bmatrix} \hat{\mathbf{F}}_{\mathrm{Bd}} \\ \mathbf{0} \end{Bmatrix}, \tag{20}$$

where the amplitudes of $\mathbf{u}$ and $\mathbf{F}$ are represented by $\hat{\mathbf{u}}$ and $\hat{\mathbf{F}}$, respectively.

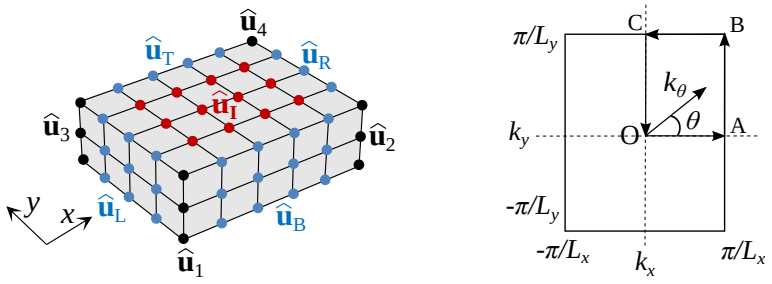

(a) A 2D unit cell.

(b) The first Brillouin zone.

Fig. 3: Illustration of the 2D periodic waveguide unit cell and the first Brillouin zone. $\hat{\mathbf{u}}$ means the amplitudes of the displacement, subscript L, R, B, T and I denote left, right, bottom, top boundary and internal DOFs. L_x and L_y are the length of the unit cell along the x and L_y direction respectively. θ is the heading angle of wave propagation. (x, y, z) are the global Cartesian coordinate system.

In Fig.3(a), a design for the 2D unit cell has been presented. The nodal DOFs in the unit cell have been partitioned into six segments, including the four corners, the left, bottom, right, top, and internal DOFs, the amplitudes of which can be described as: $\{\hat{\mathbf{u}}_{\mathrm{Bd}}^{\mathrm{T}},\ \hat{\mathbf{u}}_{\mathrm{I}}^{\mathrm{T}}\} = \{\hat{\mathbf{u}}_1^{\mathrm{T}},\ \hat{\mathbf{u}}_2^{\mathrm{T}},\ \hat{\mathbf{u}}_3^{\mathrm{T}},\ \hat{\mathbf{u}}_4^{\mathrm{T}}\ \hat{\mathbf{u}}_{\mathrm{L}}^{\mathrm{T}},\ \hat{\mathbf{u}}_{\mathrm{B}}^{\mathrm{T}},\ \hat{\mathbf{u}}_{\mathrm{R}}^{\mathrm{T}},\ \hat{\mathbf{u}}_{\mathrm{T}}^{\mathrm{T}},\ \hat{\mathbf{u}}_{\mathrm{I}}^{\mathrm{T}}\}$. It should be noted that the classification of the nodal forces is done in the same way. The periodic structures theory [58] postulates that the nodal DOFs can be represented through the utilization of the propagation constants, namely λ_x and λ_y:

$$\hat{\mathbf{u}}_2 = \lambda_x\hat{\mathbf{u}}_1,\ \hat{\mathbf{u}}_3 = \lambda_y\hat{\mathbf{u}}_1,\ \hat{\mathbf{u}}_4 = \lambda_x\lambda_y\hat{\mathbf{u}}_1,\ \hat{\mathbf{u}}_{\mathrm{R}} = \lambda_x\hat{\mathbf{u}}_{\mathrm{L}},\ \hat{\mathbf{u}}_{\mathrm{T}} = \lambda_y\hat{\mathbf{u}}_{\mathrm{B}}, \tag{21}$$

in which $\lambda_x = e^{-\mathrm{i}\kappa_x L_x}$, $\lambda_y = e^{-\mathrm{i}\kappa_y L_y}$. Within the confines of the first Brillouin zone, the wavenumbers κ_x and κ_y undergo alteration, as shown in Fig.3(b), ranging from $-\pi/L_x$ to π/L_x, and from $-\pi/L_y$ to π/L_y, respectively. On the other hand, in the case of free wave propagation, the aggregation of nodal forces from all elements linked to nodes 1, L, and B results in a null value:

$$\begin{aligned}
&\hat{\mathbf{F}}_1 + \hat{\mathbf{F}}_2\lambda_x^{-1} + \hat{\mathbf{F}}_3\lambda_y^{-1} + \hat{\mathbf{F}}_4\lambda_x^{-1}\lambda_y^{-1} = 0,\\
&\hat{\mathbf{F}}_{\mathrm{L}} + \hat{\mathbf{F}}_{\mathrm{R}}\lambda_x^{-1} = 0,\\
&\hat{\mathbf{F}}_{\mathrm{B}} + \hat{\mathbf{F}}_{\mathrm{T}}\lambda_y^{-1} = 0.
\end{aligned} \tag{22}$$

In order to solve the eigenvalue problems of Eq.20, three different solutions are proposed: the inverse form solution, the direct form solution and the Contour Integral (CI) solution. For the inverse form solution, the two wavenumbers κ_x and κ_y are given, the frequency ω needs to be calculated. For the direct form solution, the frequency ω and one wavenumber are given, the other wavenumber needs to be confirmed. For the CI solution, the frequency ω and wave propagation heading angle θ are given, the wavenumber κ_θ needs to be illustrated.

3.1. Inverse form solution

For the inverse form, the nodal DOFs of a unit cell can be represented by $\hat{\mathbf{u}}_{\mathrm{bI}}=\{\hat{\mathbf{u}}_{\mathrm{I}}^{\mathrm{T}}, \hat{\mathbf{u}}_{\mathrm{L}}^{\mathrm{T}}, \hat{\mathbf{u}}_{\mathrm{B}}^{\mathrm{T}}, \hat{\mathbf{u}}_{\mathrm{I}}^{\mathrm{T}}\}^{\mathrm{T}}$, as a result:

$$\left\{\hat{\mathbf{u}}_{\mathrm{Bd}}^{\mathrm{T}}, \hat{\mathbf{u}}_{\mathrm{I}}^{\mathrm{T}}\right\}^{\mathrm{T}} = \boldsymbol{\Lambda}_{\mathrm{R}}'\hat{\mathbf{u}}_{\mathrm{bI}}, \tag{23}$$

with

$$\boldsymbol{\Lambda}_{\mathrm{R}}' = \begin{bmatrix} \hat{\boldsymbol{\Lambda}}_{\mathrm{R}} & \mathbf{0} \\ \mathbf{0} & \mathbf{I}_{\mathrm{I}} \end{bmatrix}, \hat{\boldsymbol{\Lambda}}_{\mathrm{R}} = \begin{bmatrix} \mathbf{I}_s & \lambda_x\mathbf{I}_{\mathrm{s}} & \lambda_y\mathbf{I}_{\mathrm{s}} & \lambda_x\lambda_y\mathbf{I}_{\mathrm{s}} & \mathbf{0} & \mathbf{0} & \mathbf{0} & \mathbf{0} \\ \mathbf{0} & \mathbf{0} & \mathbf{0} & \mathbf{0} & \mathbf{I}_{\mathrm{sm}} & \mathbf{0} & \lambda_x\mathbf{I}_{\mathrm{sm}} & \mathbf{0} \\ \mathbf{0} & \mathbf{0} & \mathbf{0} & \mathbf{0} & \mathbf{0} & \mathbf{I}_{\mathrm{sn}} & \mathbf{0} & \lambda_y\mathbf{I}_{\mathrm{sn}} \end{bmatrix}^{\mathrm{T}}, \tag{24}$$

where $\mathbf{I}_{\mathrm{I}}$, $\mathbf{I}_{\mathrm{s}}$, $\mathbf{I}_{\mathrm{sn}}$ and $\mathbf{I}_{\mathrm{sm}}$ are the identity matrices of dimensions I, s, sn and sm, respectively. On the other hand, for the nodal forces:

$$\boldsymbol{\Lambda}_{\mathrm{L}}' \begin{Bmatrix} \hat{\mathbf{F}}_{\mathrm{Bd}} \\ \mathbf{0} \end{Bmatrix} = \mathbf{0}, \tag{25}$$

with

$$\boldsymbol{\Lambda}_{\mathrm{L}}' = \begin{bmatrix} \hat{\boldsymbol{\Lambda}}_{\mathrm{L}} & \mathbf{0} \\ \mathbf{0} & \mathbf{I}_{\mathrm{I}} \end{bmatrix}, \hat{\boldsymbol{\Lambda}}_{\mathrm{L}} = \begin{bmatrix} \mathbf{I}_{\mathrm{s}} & \lambda_x^{-1}\mathbf{I}_{\mathrm{s}} & \lambda_y^{-1}\mathbf{I}_{\mathrm{s}} & \lambda_x^{-1}\lambda_y^{-1}\mathbf{I}_{\mathrm{s}} & \mathbf{0} & \mathbf{0} & \mathbf{0} & \mathbf{0} \\ \mathbf{0} & \mathbf{0} & \mathbf{0} & \mathbf{0} & \mathbf{I}_{\mathrm{sm}} & \mathbf{0} & \lambda_x^{-1}\mathbf{I}_{\mathrm{sm}} & \mathbf{0} \\ \mathbf{0} & \mathbf{0} & \mathbf{0} & \mathbf{0} & \mathbf{0} & \mathbf{I}_{\mathrm{sn}} & \mathbf{0} & \lambda_y^{-1}\mathbf{I}_{\mathrm{sn}} \end{bmatrix}. \tag{26}$$

Then, submitting Eq.23 and Eq.25 into Eq.20, this yields:

$$\mathbf{\Lambda}'_{\mathrm{L}}\left(\tilde{\mathbf{K}}-\omega^2\mathbf{M}\right)\mathbf{\Lambda}'_{\mathrm{R}}\hat{\mathbf{u}}_{\mathrm{bI}}=\mathbf{0}, \tag{27}$$

which the standard, linear eigenvalue problem in ω^2 subsequently results from the following:

$$\left[\mathbf{K}^*(\lambda_x,\lambda_y)-\omega^2\mathbf{M}^*(\lambda_x,\lambda_y)\right]\hat{\mathbf{u}}_{\mathrm{bI}}=\mathbf{0}. \tag{28}$$

The magnitude of the eigenvalue conundrum is equivalent to that of $\hat{\mathbf{u}}_{\mathrm{bI}}$. The perspective of the WFEM inverse form involves the fixation of λ_x and λ_y, after which the ω are illustrated. The formation of the n-th slowness surface is established through $\omega_n^{i,j}$, in which i indicates the i-th term of wavenumber along x direction, j means the j-th term of wavenumber along y direction, n is the n-th term of frequency under i and j. The energy flow vector, also known as the Poynting vector, at a given point (κ_x, κ_y), is equal to the gradient of the slowness surface. When considering the iso-frequency contour of the slowness surface, the Poynting vector is perpendicular to the contour curves. Furthermore, a 2D representation of the slowness surface, referred to as the band structure, can be attained through plotting λ_x and λ_y along the O–A–B–C–O contour as depicted in Fig. 3(b).

3.2. Direct form solution

The direct form of the dynamic equilibrium equation will undergo a re-expression post-dynamic condensation:

$$\mathbb{D}\hat{\mathbf{u}}_{\mathrm{Bd}}=\hat{\mathbf{F}}_{\mathrm{Bd}}, \tag{29}$$

where the condensed form of the dynamic stiffness matrix is represented by $\mathbb{D}=\mathbf{D}_{\mathrm{BdBd}}-\mathbf{D}_{\mathrm{BdI}}\mathbf{D}_{\mathrm{II}}^{-1}\mathbf{D}_{\mathrm{IBd}}$, subscript Bd and I are the boundaries and internal DOFs of the unit cell respectively. After the internal DOFs condensation, the boundary nodal DOFs can be expressed as:

$$\hat{\mathbf{u}}_{\mathrm{Bd}}=\hat{\mathbf{\Lambda}}_{\mathrm{R}}\hat{\mathbf{u}}_{\mathrm{b}}, \tag{30}$$

where $\hat{\mathbf{u}}_{\mathrm{b}}=\{\hat{\mathbf{u}}_1^{\mathrm{T}},\hat{\mathbf{u}}_{\mathrm{L}}^{\mathrm{T}},\hat{\mathbf{u}}_{\mathrm{B}}^{\mathrm{T}}\}^{\mathrm{T}}$. On the other hand, the nodal forces can be written as:

$$\hat{\mathbf{\Lambda}}_{\mathrm{L}}\hat{\mathbf{F}}_{\mathrm{Bd}}=\mathbf{0}. \tag{31}$$

By incorporating Eqs.30 and 31 into Eq.29, it follows that:

$$\hat{\mathbf{\Lambda}}_{\mathrm{L}}\mathbb{D}\hat{\mathbf{\Lambda}}_{\mathrm{R}}\hat{\mathbf{u}}_{\mathrm{b}} = \mathbf{0}. \tag{32}$$

Suppose one of (λ_x, λ_y) is given (In this work λ_y is given). Subsequently, Eq.32 transforms into a quadratic eigenvalue issue with respect to λ_x, as depicted below:

$$\frac{1}{\lambda_x}\left(\lambda_x^2\mathbf{G} + \lambda_x\mathbf{H} + \mathbf{J}\right)\hat{\mathbf{u}}_{\mathrm{b}} = \mathbf{0}, \tag{33}$$

where $\mathbf{G}$, $\mathbf{H}$ and $\mathbf{J}$ are addressed in Appendix D. The solution to the eigenvalue problem of a quadratic nature can be attained through the utilization of the polyeig function. The quadratic eigen-problem in Eq.33 can be solved using the following linearization:

$$\begin{bmatrix} -\mathbf{J} & \mathbf{0} \\ \mathbf{0} & \mathbf{I} \end{bmatrix} \begin{Bmatrix} \hat{\mathbf{u}}_{\mathrm{b}} \\ \lambda_x\hat{\mathbf{u}}_{\mathrm{b}} \end{Bmatrix} = \lambda_x \begin{bmatrix} \mathbf{H} & \mathbf{G} \\ \mathbf{I} & \mathbf{0} \end{bmatrix} \begin{Bmatrix} \hat{\mathbf{u}}_{\mathrm{b}} \\ \lambda_x\hat{\mathbf{u}}_{\mathrm{b}} \end{Bmatrix}. \tag{34}$$

In this work, the wavenumber is assumed as $\kappa_y = 0$, which means $\lambda_y = 1$ and then the wave propagates along the x direction. Finally, wavenumber κ_x can be solved from Eq.34 under different frequency.

3.3. Contour Integral (CI) solution

In this part, as shown in Fig.3(b), when the wave propagation is along a heading angle θ, the wave propagation constants λ_x and λ_y can be defined as:

$$\lambda_x = \exp(-\mathrm{i}\kappa_\theta \cos(\theta) L_x),\ \ \lambda_y = \exp(-\mathrm{i}\kappa_\theta \sin(\theta) L_y), \tag{35}$$

in which κ_θ means the wavenumber along the θ direction. Then, submitting Eq.35 into Eq.32. As a result, the dynamic equilibrium equation will be reformulated in the following form:

$$\left(\hat{\mathbf{\Lambda}}_{\mathrm{L}}(\kappa_\theta, \theta)\mathbb{D}(\omega)\hat{\mathbf{\Lambda}}_{\mathrm{R}}(\kappa_\theta, \theta)\right)\hat{\mathbf{u}}_{\mathrm{b}} = \mathbf{0}. \tag{36}$$

In this work, the frequency ω and the heading angle θ are given, the eigenvalues κ_θ can be solved within a specific contour Γ:

$$\hat{\mathbb{D}}(\kappa_\theta)\hat{\mathbf{u}}_{\mathrm{b}} = \mathbf{0}, \tag{37}$$

where $\hat{\mathbb{D}}(\kappa_\theta) \in \mathbb{C}^{n,n}$, $\hat{\mathbf{u}}_{\mathrm{b}} \in \mathbb{C}^n$, n is the size of the eigenvector. The above nonlinear eigenvalues problem can be deduced using the CI method [70], which is based on the analysis of the moments

related to the matrix $\hat{\mathbb{D}}(\kappa_\theta)$:

$$\mathcal{A}_p = \frac{1}{2\pi \mathrm{i}} \int_\Gamma (\kappa_\theta)^p \hat{\mathbb{D}}(\kappa_\theta)^{-1} \hat{\mathcal{V}} \mathrm{d}\kappa_\theta, \tag{38}$$

where $p \in \mathbb{N}$, $\hat{\mathcal{V}} \in \mathbb{C}^{n,l}$ is a probe matrix which can be chosen at random practically. Inside the contour Γ, moments $\mathcal{A}_p$ includes the spectrum information of $\hat{\mathbb{D}}(\kappa_\theta)$. So as to illustrated the nonlinear eigenvalue problems, $2\overline{p}$ moments are utilized to built the block Hankel matrices $\mathcal{B}_0$ and $\mathcal{B}_1 \in \mathbb{C}^{\overline{p}n,\overline{p}l}$:

$$\mathcal{B}_0 = \begin{bmatrix} \mathcal{A}_0 & \dots & \mathcal{A}_{\overline{p}-1} \\ \vdots & \ddots & \vdots \\ \mathcal{A}_{\overline{p}-1} & \dots & \mathcal{A}_{2\overline{p}-2} \end{bmatrix}, \ \mathcal{B}_1 = \begin{bmatrix} \mathcal{A}_1 & \dots & \mathcal{A}_{\overline{p}} \\ \vdots & \ddots & \vdots \\ \mathcal{A}_{\overline{p}} & \dots & \mathcal{A}_{2\overline{p}-1} \end{bmatrix}, \tag{39}$$

in which $\overline{p} \in \mathbb{N}$, $p = 0, ..., 2\overline{p} - 1$. Then, the Singular Value Decomposition (SVD) is expressed as:

$$\mathcal{B}_0 = \mathcal{V} \Sigma \mathcal{W}^{\mathrm{H}}, \tag{40}$$

which can be used to confirm the low rank approximation:

$$\mathcal{B}_0 \approx \mathcal{V}_0 \Sigma_0 \mathcal{W}_0^{\mathrm{H}}. \tag{41}$$

Namely, a tolerance σ_{tol} is introduced. Only the m leading singular values, which corresponds the columns of $\mathcal{V}$ and $\mathcal{W}$, are reserved according to the sorting of the singular values:

$$\sigma_1 \geq \cdots \geq \sigma_m \geq \sigma_{tol} \geq \sigma_{m+1} \approx \cdots \approx 0. \tag{42}$$

Then, the eigenvalues of matrix $\hat{\mathcal{B}}$ can be calculated, whose values are same as the ones by Eq.37 inside the contour Γ, as follows:

$$\hat{\mathcal{B}} = \mathcal{V}_0^{\mathrm{H}} \mathcal{B}_1 \mathcal{W}_0 \Sigma^{-1}, \tag{43}$$

where $\hat{\mathcal{B}} \in \mathbb{C}^{m,m}$. As a result, the nonlinear eigenvalue problem in Eq.37 is reformulated in terms of a reduced sized linear eigenvalue problem with the same eigenvalues inside Γ. After the low rank decomposition, it should be noted that $m \geq n_{sol}$, where n_{sol} is assumed as the number of eigenvalues within Γ. So as to match the condition above, the number of moments and columns of the probe matrix have to be chosen as $\overline{p}l \geq n_{sol}$, where $\overline{p} \geq 1$ is necessary. At the same time, for the accuracy and stability reasons, the maximum order of the moments $2\overline{p} - 1$ must keep small. What

is more, a numerical approximation of the integral in Eq.38 is necessary. Set a parametrization of the contour as:

$$\Gamma = \gamma_0 + \gamma_1(\cos\beta + \mathrm{i}\gamma_2 \sin\beta), \tag{44}$$

where $0 \leq \beta \leq 2\pi$. Based on these circumstances, the integral is approximated by a N-point trapezoidal rule, which causes to the discrete approximation of Eq.38, one gets:

$$\mathcal{A}_p \approx \frac{\gamma_1}{S} \sum_{j=1}^{N} (\kappa_\theta)_j^p \omega_j \mathbf{X}_j, \tag{45}$$

in which $(\kappa_\theta)_j$ is the integration point along Γ, $\omega_j = (\gamma_2 \cos\beta_j + \mathrm{i}\ \sin\beta_j)$ is the weight and $\hat{\mathbb{D}}((\kappa_\theta)_j)\mathbf{X}_j = \hat{\mathcal{V}}$ is the N linear system to be deduced. In order to ensure the numerical stability, the monomial basis $((\kappa_\theta - \gamma_0)/\gamma_1)^p$ is applied in Eq.38 and Eq.45 instead of $(\kappa_\theta)^p$. The procedure above can be used to confirm the wavenumber κ_θ under the different wave propagation heading angle θ within a closed curve of the complex plane.

4. Numerical applications

The numerical investigation anchored in the SSG theory holds undeniable value in comprehending the dynamic characteristics of complex nano-sized structures. In this section, the inverse form solution, direct form solution and CI solution of the WFEM are utilized to analyze the wave propagation of three different nano-sized complex structures.

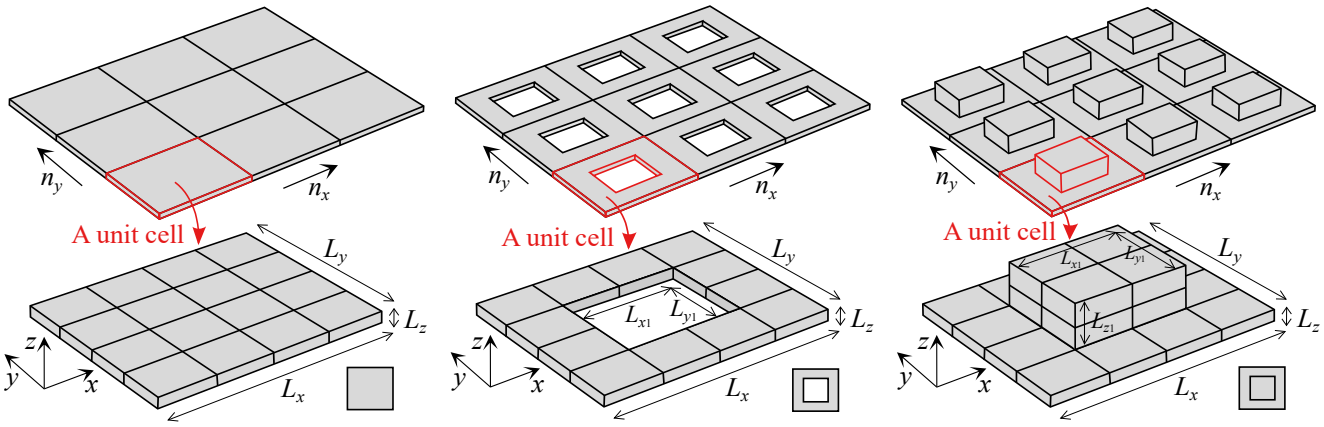

(a) Structure 1 and its unit cell. (b) Structure 2 and its unit cell. (c) Structure 3 and its unit cell.

Fig. 4: Three different periodic nano-sized structures and their meshed unit cell. Element number $n = 16$ in unit cell 1, $n = 12$ in unit cell 2 and $n = 24$ in unit cell 3.

As shown in Fig.4, three different periodic nano-sized structures constructed with unit cells are

introduced. The material of these three structures is Aluminum (Al) with $L_x = 200a_0$, $L_y = 160a_0$, $L_z = 10a_0$, $L_{x1} = 100a_0$, $L_{y1} = 80a_0$, $L_{z1} = 40a_0$ (the lattice parameter $a_0 = 4.046 \times 10^{-10}$ m). The Young's modulus, denoted as E, is determined to be 70×10^9 Pa, while the mass density, represented as ρ, is equal to 2700 kg/m^3 [71]. Additionally, the damping loss factor, designated as η, is equal to 10^{-4}. The higher-order parameters for Al [65] are depicted in Table 1.

Table 1: Higher-order parameters $a_i(eV/\text{Å})$, $b_i(eV\cdot\text{Å})$ and $c_i(eV/\text{Å})$. ($1eV = 1.602 \times 10^{-19}$ J, 1Å=10^{-10} m)

a_1	a_2	a_3	a_4	a_5	b_1	b_2	b_3	b_4	b_5
0.1407	0.0027	-0.0083	0.0966	0.2584	0.7927	0.0644	-0.1943	-0.0009	0.0009
b_6	b_7	c_1	c_2	c_3					
16.1566	48.5291	0.5041	0.3569	0.1782					

4.1. Dispersion relation

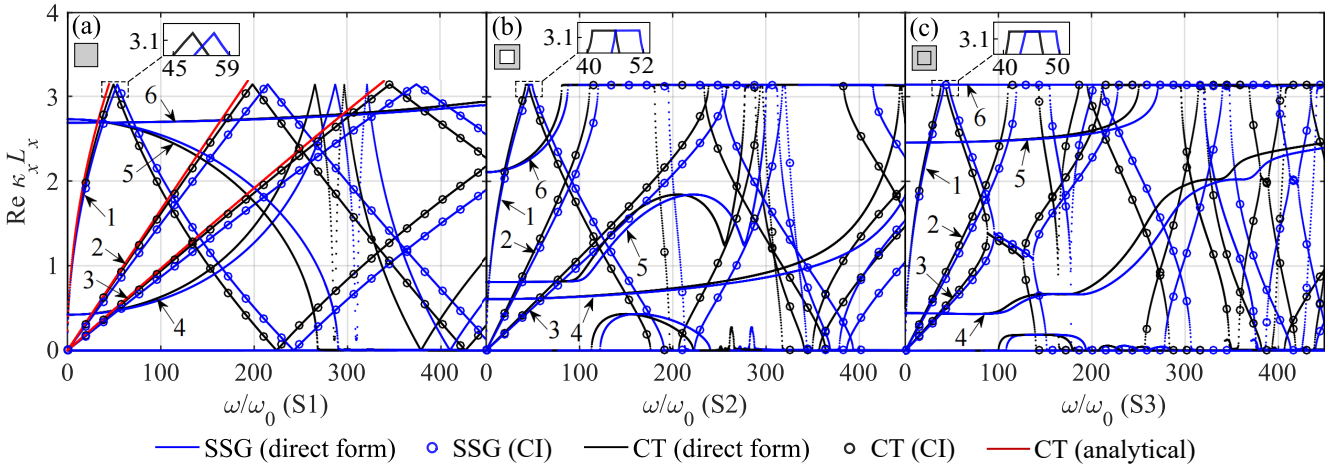

Fig. 5: Dispersion relations of three structures by the WFEM direct form and CI solutions. (a): structure 1 (S1), (b): structure 2 (S2), (c): structure 3 (S3). 1: bending, 2: shearing, 3: tension.

In this part, to analyze the wave propagation along the x direction, as illustrated in Fig.5, the dispersion relations of three waveguides are calculated using the WFEM direct form. Only the waves with positive real parts are depicted, as the waves of both negative and positive are symmetrical relative to the x-axis. The wavenumber's real part, $\text{Re}(\kappa_j)$, is defined as the phase shift per unit length. Normalization of frequency is expressed as ω/ω_0, with ω_0 representing the unit cell's first natural frequency. The blue lines signify the outcome of the SSG theory, while the black lines represent the outcome of the CT. The curve produced by the SSG theory is nearly indistinguishable from that of the CT at low frequency. However, as the frequency increases, the disparity between the results of the SSG and CT becomes increasingly apparent, which demonstrates the existence of the size effects in the nano structures clearly. According the SSG theory,

the stiffness hardening phenomena [72] appears in nano structures at the high frequency because of the higher-order parts in the strain energy density containing non classical parameters related to the long-range interactions between the microscopic particles. This significant phenomena can not be illustrated by non-local elasticity theory and surface elasticity theory.

On the other hand, in order to verify the results of WFEM direct form, the CI method under the propagation heading angle $\theta = 0$ is applied. The first three modes (bending, shearing and tension) are calculated. The curves of the first three modes by the CI match the ones by the direct form well. At the same time, the classical analytical methods for the tension, shearing and bending cases [73] are applied to validate the results of the WFEM CT in stricture 1. The results obtained from classical analytical methods are consistent with those obtained from the WFEM CT at low frequencies, demonstrating the compatibility between the two methods, but the discrepancy between them becomes bigger as the frequency increases. Here, it should be pointed out that there exist higher-order modes (e.g., modes 4, 5, 6) that the classical analytical methods can not predict. Note that the normalized first cut-off frequency for the complex thickness contractional wave 4 [55] in structure 1 is 260 by the CT, instead of 280 by the SSG. The wave 4 in structure 2 and 3 propagates continuously in the studied frequency domain. However, the classification of wave modes becomes more confusing when dealing with complex waves such as 5 and 6.

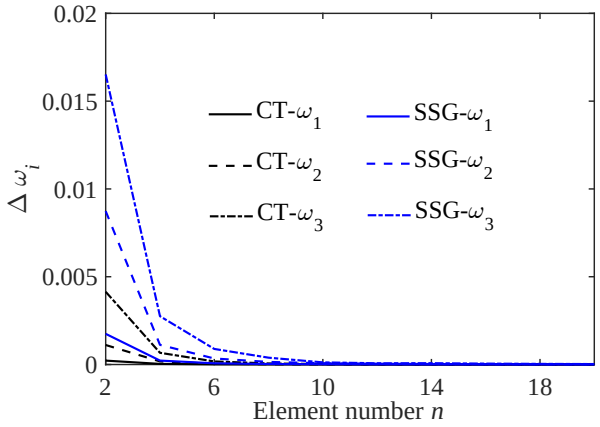

Fig. 6: Convergence of the dispersion relation in structure 1 when $\kappa_x L_x = \pi$ by the SSG and the CT.

What is more, as shown in Fig.5, the wave propagation characteristics of these three structures are different. In the structure 1, there is no band gap for the first six waves. But in the structures 2 and 3, there exist band gaps. The first band gap of wave 1 in structure 2 and 3 starts at around $\omega/\omega_0 = 40$. The first band gap range of the wave 1 in structure 2 is similar to the one in structure 3. However, the first band gap ranges of the wave 2 and 3 in structure 2 are very different to the ones in structure 3. For the higher-order wave such as the wave 6, whose first band gap starts at

around $\omega/\omega_0 = 80$ in structure 2, but $\omega/\omega_0 = 0$ in structure 3. Fig. 6 is about the convergence of the first three frequencies in structure 1 when $\kappa_x L_x = \pi$ by the SSG and the CT. The meshed element number of a unit cell in structure 1 serves as the horizontal coordinate, while the vertical coordinate represents the frequency variant: $\Delta\omega_i = |(\omega_{i(n+1)} - \omega_{i(n)})|$, where i=1, 2, 3 means the first three frequencies, n is the meshed element number of a unit cell. As illustrated in Fig. 6, there is a decline in frequency diversity as the number of elements in a unit cell increases, exhibiting a convergent trait.

4.2. Band structures

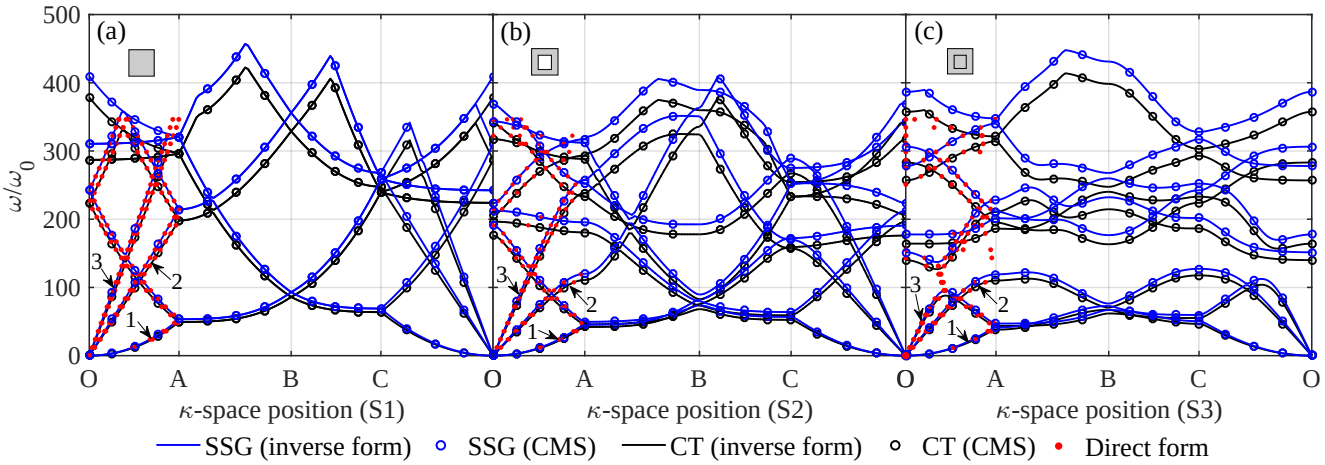

Fig. 7: Band structures of three structures by the WFEM inverse form. (a): structure 1 (S1), (b): structure 2 (S2), (c): structure 3 (S3). Red points: the first three modes from the WFEM direct form. 1: bending, 2: shearing, 3: tension.

Next, So as to illustrate the wave propagation along the x and y, the band structures of three nano structures are introduced based on the WFEM inverse form. As presented in Fig.7, the illustration depicts the five branches with the lowest normalized frequency spectrums along O-A-B-C-O. The blue lines indicate the outcomes derived from the SSG theory, while the black lines symbolize the outcomes obtained from the CT. The curve produced by the SSG is substantially similar to that produced by the CT at low frequencies. However, as the frequency increases, the distinction between the CT and the SSG becomes increasingly pronounced. On the other hand, the SSG's frequency value surpasses that of the CT at equivalent κ-space locations, which can be attributed to the fact that the dynamical equilibrium equation in the SSG theory includes non-classical components that possess higher-order parameters. As a result, the eigenvalue ω derived from the SSG theory surpasses that of the CT under the same κ-space. So as to validate the result in this part, a Component Mode Synthesis (CMS) method [74] is used. The result by WFEM

inverse form matches the CMS well. On the other hand, there is a visible band gap between the third branch and fourth branch in the structure 3. At the same time, the result shows that some parts of the waves by the direct form cannot be predicted by the inverse form, such as the waves marked in red points between the third branch and fourth branch in the structure 3. This phenomenon can be described as that in the framework of direct form, different waves can cross and switch in some certain frequency ranges.

4.3. Slowness surfaces

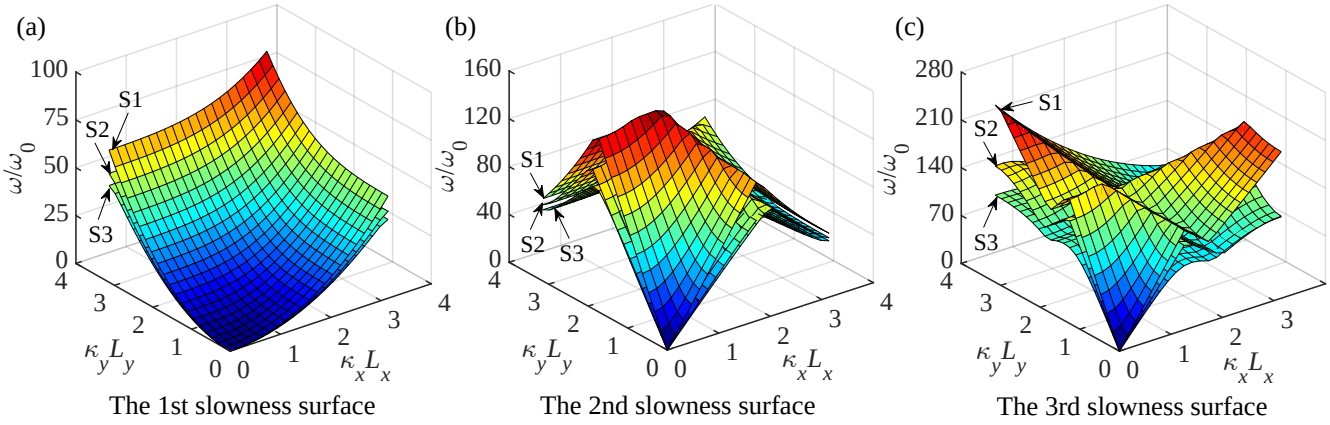

Fig. 8: The first three slowness surfaces of three structures in the first quadrant by the SSG. S1: structure 1, S2: structure 2, S3: structure 3.

In this part, the first three slowness surfaces of three structures in the first quadrant, as presented in Fig. 8, are introduced based on the SSG to study the wave propagation in the whole first Brillouin zone. The 3D surfaces exhibit symmetry in relation to κ_x and κ_y. It shows that the position of the slowness surface for structure 1 is elevated compared to structures 2 and 3, which means that the energy in the structure 1 is biggest and the energy in the structure 3 is smallest on each slowness surface at the same κ-space position. The difference between the slowness surfaces is caused by the different wave propagating and controlling capacity of each structure. The structure 1 has the high wave propagating capacity and low wave controlling capacity. The structure 3 has the low wave propagating capacity and high wave controlling capacity. The wave propagating and controlling capacity of structure 2 is between those of structures 1 and 3. On the other hand, the result shows that the 1st slowness surface of each structure is smooth, but the 2nd and 3rd slowness surfaces of each structure are rough. On the 1st slowness surface, the energy is always uniformly distributed in the first Brillouin zone. However, on the 2nd and 3rd slowness surfaces, the main energy is distributed in some specific regions. For example, the main energy is distributed along

the y-axis on the 2nd slowness surface. However, the main energy is distributed at the κ-space position A and C on the 3rd slowness surface.

4.4. Energy flow vector fields

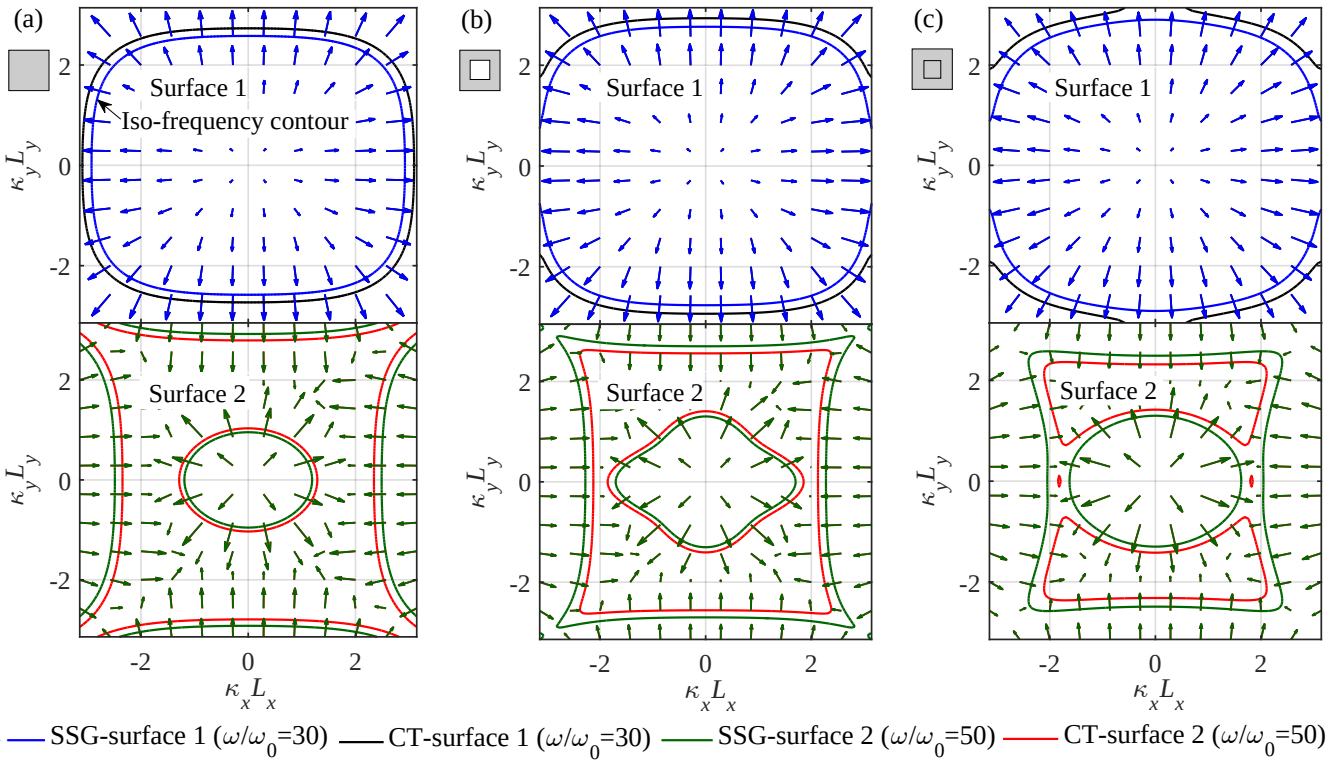

Fig. 9: The energy flow on the first two slowness surfaces of three structures by the CT and the SSG. (a): structure 1, (b): structure 2, (c): structure 3.

For the purpose of delving deeper into the wave propagation in nano structures, an investigation is conducted into the energy flow on the first two slowness surfaces of three nano structures using both the SSG and CT methods. As presented in Fig.9, the direction and length of the arrow denote the energy flow direction and gradient value respectively. The normalized frequencies of the iso-frequency contours are chosen as 30 and 50 on the first and second slowness surfaces respectively. The propagation of a plane wave is presented by the wave number κ_θ under the heading angle θ. The arrows from the SSG and the CT almost overlap on the xy plane, which means that the direction and gradient of energy flow projected onto the xy plane by the SSG are essentially equivalent as that by the CT. On the first slowness surface, the wave propagates in all directions. The iso-frequency contour posited by the SSG is situated within the one determined by the CT, indicating that the κ_θ computed by the SSG is of a lesser magnitude than that calculated by the CT for the same heading angle θ. On the second slowness surface, the energy propagates outward in the middle part, but inward at the edge. The position of the iso-frequency contour as

determined by the SSG lies exterior to that of the CT at the periphery, yet it lies interior to the contour established by the CT in the central region.

On the other hand, when it comes to low frequency waves, the wave propagation properties of the three structures bear a remarkable resemblance to one another. However, at high frequency, the wave propagation of three structures are different, which can be clearly observed in Fig.9: the range of energy that propagates outward in the structure 3 is the largest, but the smallest in the structure 1 under the same theory. Additionally, the SSG theory encompasses higher-order parameters that showcase non-local properties, thereby inducing a "hardening" effect on the nano structure. As a result, the wave propagation range experiences a transformation.

5. Conclusions

In this paper,the SSG theory, which is integrated with the WFEM, is utilized to conduct a wave propagation analysis of three complex nano structures. In order to accomplish the numerical modeling, firstly, the constitutive relations of the three-dimensional nano-sized structure are confirmed through the SSG. The displacement field is determined through the utilization of six quintic Hermite polynomial interpolating functions. The calculation of the weak form, inclusive of the element matrices, is performed by employing Hamilton's principle.

Subsequently, the dispersion relations for three nano structures are illustrated by the WFEM direct form solution and the Contour Integral (CI) solution respectively. The advantage of the WFEM is that it can predict the higher-order waves in nano-structures which cannot be solved by the analytical solution. It shows that the results of the first three modes by the direct form solution confirm the ones by the CI solution under the heading angle $\theta = 0$. The presence of non-classical components featuring higher-order parameters within SSG can induce special stiffness-hardening within nano-sized structures. The wave propagation characteristics of these three nano structures are different. In the structure 1, there is no band gap for the first six waves. But in the structures 2 and 3, there exist band gaps.

Furthermore, the band structures of three nano structures are confirmed through the WFEM inverse form solution respectively. The comparative analysis between the SSG and CT band structure curves reveals that the former exhibits close proximity to the latter at lower frequencies. However, the difference between the two curves becomes increasingly pronounced as the frequency increases. The frequency by the SSG is bigger than the CT under the same κ-space point. Some parts of the waves by the direct form cannot be predicted by the inverse form, such as the connection waves between the third branch and fourth branch in the structure 3.

Lastly, the discussion pertaining to the energy flow and the slowness surfaces of three nano structures is conducted. Results obtained show that the slowness surface position of structure 1 is higher than structures 2 and 3, which means that the energy in the structure 1 is biggest and the energy in the structure 3 is smallest on each slowness surface under same κ-space. The structure 1 has the high wave propagating capacity and low wave controlling capacity, while the structure 3 has the low wave propagating capacity and high wave controlling capacity. Furthermore, due to the existence of the "hardening" phenomena in the nano structures through the SSG, the wave propagation range experiences a transformation.

Acknowledgements

The authors acknowledge the financial support of the Italian Ministry of University and Research (MUR), Research Grant PRIN 2020 No. 2020EBLPLS on "Opportunities and challenges of nanotechnology in advanced and green construction materials", CUP code: B67G21000110001.

Appendix A. Definition of matrices $\boldsymbol{\Psi_1}$, $\boldsymbol{\Psi_2}$ and $\boldsymbol{\Psi_3}$ in Eq.3

$$\boldsymbol{\Psi}_1 = \begin{bmatrix} \partial_x & 0 & 0 & 0 & \partial_z & 0 \\ 0 & \partial_y & 0 & \partial_z & 0 & \partial_y \\ 0 & 0 & \partial_z & \partial_y & \partial_x & \partial_x \end{bmatrix}^{\mathrm{T}}, \ \boldsymbol{\Psi}_2 = \begin{bmatrix} \mathbf{e}_1 & \mathbf{0} & \mathbf{0} \\ \mathbf{0} & \mathbf{e}_1 & \mathbf{0} \\ \mathbf{0} & \mathbf{0} & \mathbf{e}_1 \end{bmatrix} \otimes \{\partial_{xx}, \partial_{yy}, \partial_{zz}, 2\partial_{xy}, 2\partial_{xz}, 2\partial_{yz}\}^{\mathrm{T}},$$

$$\boldsymbol{\Psi}_3 = \begin{bmatrix} \mathbf{e}_2 & \mathbf{0} & \mathbf{0} \\ \mathbf{0} & \mathbf{e}_2 & \mathbf{0} \\ \mathbf{0} & \mathbf{0} & \mathbf{e}_2 \end{bmatrix} \otimes \{\partial_{xxx}, \partial_{yyy}, \partial_{zzz}, 3\partial_{xxy}, 3\partial_{xxz}, 3\partial_{yyx}, 3\partial_{yyz}, 3\partial_{zzx}, 3\partial_{zzy}, 6\partial_{xyz}\}^{\mathrm{T}},$$ where symbol $\otimes$ indicates the Kronecker product, $\mathbf{e}_{1(6\times1)}$ and $\mathbf{e}_{2(10\times1)}$ are the vectors of ones.

Appendix B. Definition of matrices $\mathbf{L_{(6\times6)}}$, $\mathbf{A_{(18\times18)}}$, $\mathbf{B_{(30\times30)}}$ and $\mathbf{C_{(6\times30)}}$ in Eq.4

The matrix $\mathbf{L}_{(6\times6)}$: $\mathbf{L}_{(1,1)} = \mathbf{L}_{(2,2)} = \mathbf{L}_{(3,3)} = \lambda + 2\mu$, $\mathbf{L}_{(4,4)} = \mathbf{L}_{(5,5)} = \mathbf{L}_{(6,6)} = \mu$, $\mathbf{L}_{(1,2)} = \mathbf{L}_{(2,1)} = \mathbf{L}_{(1,3)} = \mathbf{L}_{(3,1)} = \mathbf{L}_{(2,3)} = \mathbf{L}_{(3,2)} = \lambda$.

The matrix $\mathbf{A}_{(18\times18)}$: $\mathbf{A}_{(1,1)} = 2(a_1 + a_2 + a_3 + a_4 + a_5)$, $\mathbf{A}_{(1,2)} = \mathbf{A}_{(2,1)} = a_2 + 2a_3$, $\mathbf{A}_{(1,3)} = \mathbf{A}_{(3,1)} = a_2 + 2a_3$, $\mathbf{A}_{(1,4)} = \mathbf{A}_{(4,1)} = (2a_1 + a_2)/2$, $\mathbf{A}_{(1,5)} = \mathbf{A}_{(5,1)} = (2a_1 + a_2)/2$, $\mathbf{A}_{(2,2)} = 2(a_3 + a_4)$, $\mathbf{A}_{(2,3)} = \mathbf{A}_{(3,2)} = 2(a_3)$, $\mathbf{A}_{(2,4)} = \mathbf{A}_{(4,2)} = (a_2 + 2a_5)/2$, $\mathbf{A}_{(2,5)} = \mathbf{A}_{(5,2)} = (a_2)/2$, $\mathbf{A}_{(3,3)} = 2(a_3 + a_4)$, $\mathbf{A}_{(3,4)} = \mathbf{A}_{(4,3)} = a_2/2$, $\mathbf{A}_{(3,5)} = \mathbf{A}_{(5,3)} = (a_2 + 2a_5)/2$, $\mathbf{A}_{(4,4)} = (a_1 + 2a_4 + a_5)/2$, $\mathbf{A}_{(4,5)} = \mathbf{A}_{(5,4)} = (a_1)/2$, $\mathbf{A}_{(5,5)} = (a_1 + 2a_4 + a_5)/2$, $\mathbf{A}_{(6,6)} = 2(a_1 + a_2 + a_3 + a_4 + a_5)$, $\mathbf{A}_{(6,7)} = \mathbf{A}_{(7,6)} = a_2 + 2a_3$, $\mathbf{A}_{(6,8)} = \mathbf{A}_{(8,6)} = a_2 + 2a_3$, $\mathbf{A}_{(6,9)} = \mathbf{A}_{(9,6)} = (2a_2 + a_2)/2$, $\mathbf{A}_{(6,10)} = \mathbf{A}_{(10,6)} = (2a_2 + a_2)/2$,

$\mathbf{A}_{(7,7)} = 2(a_3{+}a_4)$, $\mathbf{A}_{(7,8)} = \mathbf{A}_{(8,7)} = 2(a_3)$, $\mathbf{A}_{(7,9)} = \mathbf{A}_{(9,7)} = (a_2{+}2a_5)/2$, $\mathbf{A}_{(7,10)} = \mathbf{A}_{(10,7)} = (a_2)/2$, $\mathbf{A}_{(8,8)} = 2(a_3{+}a_4)$, $\mathbf{A}_{(8,9)} = \mathbf{A}_{(9,8)} = a_2/2$, $\mathbf{A}_{(8,10)} = \mathbf{A}_{(10,8)} = (a_2{+}2a_5)/2$, $\mathbf{A}_{(9,9)} = (a_1{+}2a_4{+}a_5)/2$, $\mathbf{A}_{(9,10)} = \mathbf{A}_{(10,9)} = (a_1)/2$, $\mathbf{A}_{(10,10)} = (a_1 + 2a_4 + a_5)/2$, $\mathbf{A}_{(11,11)} = 2(a_1 + a_2 + a_3 + a_4 + a_5)$, $\mathbf{A}_{(11,12)} = \mathbf{A}_{(12,11)} = a_2 + 2a_3$, $\mathbf{A}_{(11,13)} = \mathbf{A}_{(13,11)} = a_2 + 2a_3$, $\mathbf{A}_{(11,14)} = \mathbf{A}_{(14,11)} = (2a_2 + a_2)/2$, $\mathbf{A}_{(11,15)} = \mathbf{A}_{(15,11)} = (2a_2 + a_2)/2$, $\mathbf{A}_{(12,12)} = 2(a_3 + a_4)$, $\mathbf{A}_{(12,13)} = \mathbf{A}_{(13,12)} = 2(a_3)$, $\mathbf{A}_{(12,14)} = \mathbf{A}_{(14,12)} = (a_2{+}2a_5)/2$, $\mathbf{A}_{(12,15)} = \mathbf{A}_{(15,12)} = (a_2)/2$, $\mathbf{A}_{(13,13)} = 2(a_3{+}a_4)$, $\mathbf{A}_{(13,14)} = \mathbf{A}_{(14,13)} = a_2/2$, $\mathbf{A}_{(13,15)} = \mathbf{A}_{(15,13)} = (a_2 + 2a_5)/2$, $\mathbf{A}_{(14,14)} = (a_1 + 2a_4 + a_5)/2$, $\mathbf{A}_{(14,15)} = \mathbf{A}_{(15,14)} = (a_1)/2$, $\mathbf{A}_{(15,15)} = (a_1 + 2a_4 + a_5)/2$, $\mathbf{A}_{(16,16)} = a_4$, $\mathbf{A}_{(16,17)} = \mathbf{A}_{(17,16)} = (a_5)/2$, $\mathbf{A}_{(16,18)} = \mathbf{A}_{(18,16)} = (a_5)/2$, $\mathbf{A}_{(17,17)} = a_4$, $\mathbf{A}_{(17,18)} = \mathbf{A}_{(18,17)} = (a_5)/2$, $\mathbf{A}_{(18,18)} = a_4$.

The matrix $\mathbf{B}_{(30\times30)}$: $\mathbf{B}_{(1,1)} = 2(b_1{+}b_2{+}b_3{+}b_4{+}b_5{+}b_6{+}b_7)$, $\mathbf{B}_{(1,6)} = \mathbf{B}_{(6,1)} = (2b_1{+}b_3{+}2b_4{+}2b_5)/3$, $\mathbf{B}_{(1,8)} = \mathbf{B}_{(8,1)} = (2b_1{+}b_3{+}2b_4{+}2b_5)/3$, $\mathbf{B}_{(1,12)} = \mathbf{B}_{(12,1)} = 2b_1$, $\mathbf{B}_{(1,14)} = \mathbf{B}_{(14,1)} = (2b_1{+}2b_2{+}b_3)/3$, $\mathbf{B}_{(1,19)} = \mathbf{B}_{(19,1)} = 2b_1/3$, $\mathbf{B}_{(1,23)} = \mathbf{B}_{(23,1)} = 2b_1$, $\mathbf{B}_{(1,25)} = \mathbf{B}_{(25,1)} = (2b_1 + 2b_2 + b_3)/3$, $\mathbf{B}_{(1,27)} = \mathbf{B}_{(27,1)} = 2b_1/3$, $\mathbf{B}_{(2,2)} = 2(b_5 + b_6)$, $\mathbf{B}_{(2,4)} = \mathbf{B}_{(4,2)} = (b_3 + 2b_5)/3$, $\mathbf{B}_{(2,9)} = \mathbf{B}_{(9,2)} = 2b_5/3$, $\mathbf{B}_{(2,11)} = \mathbf{B}_{(11,2)} = 2b_4$, $\mathbf{B}_{(2,16)} = \mathbf{B}_{(16,2)} = (b_3 + 2b_4 + 2b_7)/3$, $\mathbf{B}_{(2,18)} = \mathbf{B}_{(18,2)} = 2b_4/3$, $\mathbf{B}_{(2,30)} = \mathbf{B}_{(30,2)} = b_3/6$, $\mathbf{B}_{(3,3)} = 2(b_5 + b_6)$, $\mathbf{B}_{(3,5)} = \mathbf{B}_{(5,3)} = (b_3 + 2b_5)/3$, $\mathbf{B}_{(3,7)} = \mathbf{B}_{(7,3)} = 2b_5/3$, $\mathbf{B}_{(3,20)} = \mathbf{B}_{(20,3)} = b_3/6$, $\mathbf{B}_{(3,21)} = \mathbf{B}_{(21,3)} = 2b_4$, $\mathbf{B}_{(3,26)} = \mathbf{B}_{(26,3)} = 2b_4/3$, $\mathbf{B}_{(3,28)} = \mathbf{B}_{(28,3)} = (b_3 + 2b_4 + 2b_7)/3$, $\mathbf{B}_{(4,4)} = 2(2b_2 + b_3 + b_5 + 3b_6 + 2b_7)/9$, $\mathbf{B}_{(4,9)} = \mathbf{B}_{(9,4)} = (b_3 + 2b_5)/3/3$, $\mathbf{B}_{(4,11)} = \mathbf{B}_{(11,4)} = (b_3 + 2b_4 + 2b_7)/3$, $\mathbf{B}_{(4,16)} = \mathbf{B}_{(16,4)} = 2(2b_2 + b_3 + b_4)/9$, $\mathbf{B}_{(4,18)} = \mathbf{B}_{(18,4)} = (b_3 + 2b_4)/9$, $\mathbf{B}_{(4,30)} = \mathbf{B}_{(30,4)} = (2b_2{+}b_3)/18$, $\mathbf{B}_{(5,5)} = 2(2b_2{+}b_3{+}b_5{+}3b_6{+}2b_7)/9$, $\mathbf{B}_{(5,7)} = \mathbf{B}_{(7,5)} = (b_3{+}2b_5)/3/3$, $\mathbf{B}_{(5,19)} = \mathbf{B}_{(19,5)} = (2b_2 + b_3)/18$, $\mathbf{B}_{(5,20)} = \mathbf{B}_{(20,5)} = (b_3 + 2b_4 + 2b_7)/3$, $\mathbf{B}_{(5,25)} = \mathbf{B}_{(25,5)} = (b_3 + 2b_4)/9$, $\mathbf{B}_{(5,27)} = \mathbf{B}_{(27,5)} = 2(2b_2 + b_3 + b_4)/9$, $\mathbf{B}_{(6,6)} = 2(b_2 + 3b_6 + b_7)/9 + 2(b_1 + b_4 + b_5)/9$, $\mathbf{B}_{(6,8)} = \mathbf{B}_{(8,6)} = 2(b_1 + b_4 + b_5)/9$, $\mathbf{B}_{(6,12)} = \mathbf{B}_{(12,6)} = (2b_1 + 2b_2 + b_3)/3$, $\mathbf{B}_{(6,14)} = \mathbf{B}_{(14,6)} = 2(b_1 + b_3 + 2b_7)/9$, $\mathbf{B}_{(6,19)} = \mathbf{B}_{(19,6)} = (2b_1 + b_3)/9$, $\mathbf{B}_{(6,23)} = \mathbf{B}_{(23,6)} = 2b_1/3$, $\mathbf{B}_{(6,25)} = \mathbf{B}_{(25,6)} = (2b_1{+}b_3)/9$, $\mathbf{B}_{(6,27)} = \mathbf{B}_{(27,6)} = 2(b_1{+}b_2)/9$, $\mathbf{B}_{(7,7)} = 2(b_5{+}3b_6)/9$, $\mathbf{B}_{(7,20)} = \mathbf{B}_{(20,7)} = (b_3{+}4b_7)/18$, $\mathbf{B}_{(7,21)} = \mathbf{B}_{(21,7)} = 2b_4/3$, $\mathbf{B}_{(7,26)} = \mathbf{B}_{(26,7)} = 2(b_4 + b_7)/9$, $\mathbf{B}_{(7,28)} = \mathbf{B}_{(28,7)} = (b_3 + 2b_4)/9$, $\mathbf{B}_{(8,8)} = 2(b_2{+}3b_6{+}b_7)/9{+}2(b_1{+}b_4{+}b_5)/9$, $\mathbf{B}_{(8,12)} = \mathbf{B}_{(12,8)} = 2b_1/3$, $\mathbf{B}_{(8,14)} = \mathbf{B}_{(14,8)} = (2b_1{+}b_3)/9$, $\mathbf{B}_{(8,19)} = \mathbf{B}_{(19,8)} = 2(b_1 + b_2)/9$, $\mathbf{B}_{(8,23)} = \mathbf{B}_{(23,8)} = (2b_1 + 2b_2 + b_3)/3$, $\mathbf{B}_{(8,25)} = \mathbf{B}_{(25,8)} = 2(b_1 + b_3 + 2b_7)/9$, $\mathbf{B}_{(8,27)} = \mathbf{B}_{(27,8)} = (2b_1 + b_3)/9$, $\mathbf{B}_{(9,9)} = 2(b_5 + 3b_6)/9$, $\mathbf{B}_{(9,11)} = \mathbf{B}_{(11,9)} = 2b_4/3$, $\mathbf{B}_{(9,16)} = \mathbf{B}_{(16,9)} = (b_3 + 2b_4)/9$, $\mathbf{B}_{(9,18)} = \mathbf{B}_{(18,9)} = 2(b_4 + b_7)/9$, $\mathbf{B}_{(9,30)} = \mathbf{B}_{(30,9)} = (b_3 + 4b_7)/18$, $\mathbf{B}_{(10,10)} = 2(b_2 + 3b_6 + b_7)/9/2$, $\mathbf{B}_{(10,13)} = \mathbf{B}_{(13,10)} = b_3/6$, $\mathbf{B}_{(10,15)} = \mathbf{B}_{(15,10)} = (b_3 + 4b_7)/18$, $\mathbf{B}_{(10,17)} = \mathbf{B}_{(17,10)} = (2b_2 + b_3)/18$, $\mathbf{B}_{(10,22)} = \mathbf{B}_{(22,10)} = b_3/6$, $\mathbf{B}_{(10,24)} = \mathbf{B}_{(24,10)} = (b_3 + 4b_7)/18$, $\mathbf{B}_{(10,29)} = \mathbf{B}_{(29,10)} = (2b_2{+}b_3)/18$, $\mathbf{B}_{(11,11)} = 2(b_5{+}b_6)$, $\mathbf{B}_{(11,16)} = \mathbf{B}_{(16,11)} = (b_3{+}2b_5)/3$, $\mathbf{B}_{(11,18)} = \mathbf{B}_{(18,11)} = 2b_5/3$, $\mathbf{B}_{(11,30)} = \mathbf{B}_{(30,11)} = b_3/6$, $\mathbf{B}_{(12,12)} = 2(b_1 + b_2 + b_3 + b_4 + b_5 + b_6 + b_7)$, $\mathbf{B}_{(12,14)} =$

$\mathbf{B}_{(14,12)} = (2b_1 + b_3 + 2b_4 + 2b_5)/3/3$, $\mathbf{B}_{(12,19)} = \mathbf{B}_{(19,12)} = (2b_1 + b_3 + 2b_4 + 2b_5)/3/3$, $\mathbf{B}_{(12,23)} = \mathbf{B}_{(23,12)} = 2b_1$, $\mathbf{B}_{(12,25)} = \mathbf{B}_{(25,12)} = 2b_1/3$, $\mathbf{B}_{(12,27)} = \mathbf{B}_{(27,12)} = (2b_1+2b_2+b_3)/3$, $\mathbf{B}_{(13,13)} = 2(b_5+b_6)$, $\mathbf{B}_{(13,15)} = \mathbf{B}_{(15,13)} = 2b_5/3$, $\mathbf{B}_{(13,17)} = \mathbf{B}_{(17,13)} = (b_3 + 2b_5)/3$, $\mathbf{B}_{(13,22)} = 2\mathbf{B}_{(22,13)} = b_4$, $\mathbf{B}_{(13,24)} = \mathbf{B}_{(24,13)} = 2b_4/3$, $\mathbf{B}_{(13,29)} = \mathbf{B}_{(29,13)} = (b_3+2b_4+2b_7)/3$, $\mathbf{B}_{(14,14)} = 2(b_2+3b_6+b_7)/9+2(b_1+b_4+b_5)/9$, $\mathbf{B}_{(14,19)} = \mathbf{B}_{(19,14)} = 2(b_1 + b_4 + b_5)/9$, $\mathbf{B}_{(14,23)} = \mathbf{B}_{(23,14)} = 4b_1/3$, $\mathbf{B}_{(14,25)} = \mathbf{B}_{(25,14)} = 2(b_1 + b_2)/9$, $\mathbf{B}_{(14,27)} = \mathbf{B}_{(27,14)} = (2b_1 + b_3)/9$, $\mathbf{B}_{(15,15)} = 2(b_5 + 3b_6)/9$, $\mathbf{B}_{(15,17)} = \mathbf{B}_{(17,15)} = (b_3 + 2b_5)/3/3$, $\mathbf{B}_{(15,22)} = \mathbf{B}_{(22,15)} = 2b_4/3$, $\mathbf{B}_{(15,24)} = \mathbf{B}_{(24,15)} = 2(b_4 + b_7)/9$, $\mathbf{B}_{(15,29)} = \mathbf{B}_{(29,15)} = (b_3 + 2b_4)/9$, $\mathbf{B}_{(16,16)} = 2(2b_2 + b_3 + b_5 + 3b_6 + 2b_7)/9$, $\mathbf{B}_{(16,18)} = \mathbf{B}_{(18,16)} = (b_3 + 2b_5)/3/3$, $\mathbf{B}_{(16,30)} = \mathbf{B}_{(30,16)} = (2b_2 + b_3)/18$, $\mathbf{B}_{(17,17)} = 2(2b_2 + b_3 + b_5 + 3b_6 + 2b_7)/9$, $\mathbf{B}_{(17,22)} = \mathbf{B}_{(22,17)} = (b_3 + 2b_4 + 2b_7)/3$, $\mathbf{B}_{(17,24)} = \mathbf{B}_{(24,17)} = (b_3 + 2b_4)/9$, $\mathbf{B}_{(17,29)} = \mathbf{B}_{(29,17)} = 2(2b_2 + b_3 + b_4)/9$, $\mathbf{B}_{(18,18)} = 2(b_1 + b_2 + b_3 + b_4 + b_5 + b_6 + b_7)$, $\mathbf{B}_{(18,30)} = \mathbf{B}_{(30,18)} = (b_3 + 4b_7)/18$, $\mathbf{B}_{(19,19)} = 2(b_2 + 3b_6 + b_7)/9 + 2(b_1 + b_4 + b_5)/9$, $\mathbf{B}_{(19,23)} = \mathbf{B}_{(23,19)} = (2b_1 + 2b_2 + b_3)/3$, $\mathbf{B}_{(19,25)} = \mathbf{B}_{(25,19)} = (2b_1 + b_3)/9$, $\mathbf{B}_{(19,27)} = \mathbf{B}_{(27,19)} = 2(b_1 + b_3 + 2b_7)/9$, $\mathbf{B}_{(20,20)} = 2(b_2 + 3b_6 + b_7)/9/3$, $\mathbf{B}_{(20,21)} = \mathbf{B}_{(21,20)} = b_3/6$, $\mathbf{B}_{(20,26)} = \mathbf{B}_{(26,20)} = (b_3+4b_7)/18$, $\mathbf{B}_{(20,28)} = \mathbf{B}_{(28,20)} = (2b_2+b_3)/18$, $\mathbf{B}_{(21,21)} = 2(b_5+b_6)$, $\mathbf{B}_{(21,26)} = \mathbf{B}_{(26,21)} = 2b_5/3$, $\mathbf{B}_{(21,28)} = \mathbf{B}_{(28,21)} = (b_3 + 2b_5)/3$, $\mathbf{B}_{(22,22)} = 2(b_5 + b_6)$, $\mathbf{B}_{(22,24)} = \mathbf{B}_{(24,22)} = 2b_5/3$, $\mathbf{B}_{(22,29)} = \mathbf{B}_{(29,22)} = 2(b_3 + 2b_5)/3$, $\mathbf{B}_{(23,23)} = 2(b_1 + b_2 + b_3 + b_4 + b_5 + b_6 + b_7)$, $\mathbf{B}_{(23,25)} = \mathbf{B}_{(25,23)} = 2(2b_1 + b_3 + 2b_4 + 2b_5)/3$, $\mathbf{B}_{(23,27)} = \mathbf{B}_{(27,23)} = (2b_1 + b_3 + 2b_4 + 2b_5)/3/3$, $\mathbf{B}_{(24,24)} = 2(b_5 + 3b_6)/9$, $\mathbf{B}_{(24,29)} = \mathbf{B}_{(29,24)} = (b_3 + 2b_5)/3/3$, $\mathbf{B}_{(25,25)} = 2(b_2 + 3b_6 + b_7)/9 + 2(b_1 + b_4 + b_5)/9$, $\mathbf{B}_{(26,26)} = 2(b_5+3b_6)/9$, $\mathbf{B}_{(27,27)} = 2(b_2+3b_6+b_7)/9+2(b_1+b_4+b_5)/9$, $\mathbf{B}_{(28,28)} = 2(2b_2+b_3+b_5+3b_6+2b_7)/9$, $\mathbf{B}_{(29,29)} = 2(2b_2 + b_3 + b_5 + 3b_6 + 2b_7)/9$, $\mathbf{B}_{(30,30)} = 2(b_2 + 3b_6 + b_7)/9/3$.

The matrix $\mathbf{C}_{(6\times30)}$: $\mathbf{C}_{(1,1)} = c_1 + c_2 + c_3$, $\mathbf{C}_{(1,6)} = (c_1 + c_3)/3$, $\mathbf{C}_{(1,8)} = (c_1 + c_3)/3$, $\mathbf{C}_{(1,12)} = c_1$, $\mathbf{C}_{(1,14)} = (c_1 + c_2)/3$, $\mathbf{C}_{(1,19)} = c_1$, $\mathbf{C}_{(1,23)} = c_1$, $\mathbf{C}_{(1,25)} = (c_1 + c_2)/3$, $\mathbf{C}_{(1,27)} = c_1$, $\mathbf{C}_{(2,1)} = c_1$, $\mathbf{C}_{(2,6)} = (c_1 + c_2)/3$, $\mathbf{C}_{(2,8)} = c_1$, $\mathbf{C}_{(2,12)} = c_1 + c_2 + c_3$, $\mathbf{C}_{(2,19)} = (c_1 + c_3)/3$, $\mathbf{C}_{(2,23)} = c_1$, $\mathbf{C}_{(2,25)} = c_1$, $\mathbf{C}_{(2,27)} = (c_1 + c_2)/3$, $\mathbf{C}_{(3,1)} = c_1$, $\mathbf{C}_{(3,6)} = c_1$, $\mathbf{C}_{(3,8)} = (c_1 + c_2)/3$, $\mathbf{C}_{(3,12)} = c_1$, $\mathbf{C}_{(3,14)} = c_1$, $\mathbf{C}_{(3,19)} = (c_1 + c_2)/3$, $\mathbf{C}_{(3,23)} = c_1 + c_2 + c_3$, $\mathbf{C}_{(3,25)} = (c_1 + c_3)/3$, $\mathbf{C}_{(3,27)} = (c_1 + c_3)/3$, $\mathbf{C}_{(4,10)} = c_2/6$, $\mathbf{C}_{(4,13)} = c_3/2$, $\mathbf{C}_{(4,15)} = c_3/2$, $\mathbf{C}_{(4,17)} = (2c_2 + c_3)/6$, $\mathbf{C}_{(4,22)} = c_3/2$, $\mathbf{C}_{(4,24)} = c_3/2$, $\mathbf{C}_{(4,29)} = (2c_2 + c_3)/6$, $\mathbf{C}_{(5,3)} = c_3/2$, $\mathbf{C}_{(5,5)} = (2c_2 + c_3)/6$, $\mathbf{C}_{(5,7)} = c_3/2$, $\mathbf{C}_{(5,20)} = c_2/6$, $\mathbf{C}_{(5,21)} = c_3/2$, $\mathbf{C}_{(5,26)} = c_3/2$, $\mathbf{C}_{(5,28)} = (2c_2 + c_3)/6$, $\mathbf{C}_{(6,2)} = c_3/2$, $\mathbf{C}_{(6,4)} = (2c_2 + c_3)/6$, $\mathbf{C}_{(6,9)} = c_3/2$, $\mathbf{C}_{(6,11)} = c_3/2$, $\mathbf{C}_{(6,18)} = c_3/2$, $\mathbf{C}_{(6,30)} = c_2/6$. Here, it should be noted that the values of the rest parts that not mentioned in the matrices $\mathbf{L}$, $\mathbf{A}$, $\mathbf{B}$ and $\mathbf{C}$ are 0.

Appendix C. Definition of $\mathbf{S_1^0(\overline{x})}$, $\mathbf{S_1^1(\overline{x})}$, $\mathbf{S_1^2(\overline{x})}$, $\mathbf{S_2^0(\overline{x})}$, $\mathbf{S_2^1(\overline{x})}$ and $\mathbf{S_2^2(\overline{x})}$ in Eq.9

$\mathrm{S}_1^0(\overline{x})=5\overline{x}^3/(8l_e^3)-15\overline{x}/(16l_e)-3\overline{x}^5/(16l_e^5)+1/2$, $\mathrm{S}_1^1(\overline{x})=5l_e/16-7\overline{x}/16-3\overline{x}^2/(8l_e)+5\overline{x}^3/(8l_e^2)+\overline{x}^4/(16l_e^3)-3\overline{x}^5/(16l_e^4)$, $\mathrm{S}_1^2(\overline{x})=l_e^2/16-l_e\overline{x}/16-\overline{x}^2/8+\overline{x}^3/(8l_e)+\overline{x}^4/(16l_e^2)-\overline{x}^5/(16l_e^3)$, $\mathrm{S}_2^0(\overline{x})=15\overline{x}/(16l_e)-5\overline{x}^3/(8l_e^3)+3\overline{x}^5/(16l_e^5)+1/2$, $\mathrm{S}_2^1(\overline{x})=3\overline{x}^2/(8l_e)-7\overline{x}/16-5l_e/16+5\overline{x}^3/(8l_e^2)-\overline{x}^4/(16l_e^3)-3\overline{x}^5/(16l_e^4)$, $\mathrm{S}_2^2(\overline{x})=l_e\overline{x}/16+l_e^2/16-\overline{x}^2/8-\overline{x}^3/(8l_e)+\overline{x}^4/(16l_e^2)+\overline{x}^5/(16l_e^3)$.

Appendix D. Expressions of the coefficients G, H and J in Eq.33

$$\mathbf{G}=\begin{bmatrix}\mathbf{G}_{11} & \mathbf{G}_{1\mathrm{L}} & \mathbf{G}_{1\mathrm{B}}\\ \mathbf{G}_{\mathrm{L}1} & \mathbf{G}_{\mathrm{LL}} & \mathbf{G}_{\mathrm{LB}}\\ \mathbf{G}_{\mathrm{B}1} & \mathbf{G}_{\mathrm{BL}} & \mathbf{G}_{\mathrm{BB}}\end{bmatrix},\ \mathbf{H}=\begin{bmatrix}\mathbf{H}_{11} & \mathbf{H}_{1\mathrm{L}} & \mathbf{H}_{1\mathrm{B}}\\ \mathbf{H}_{\mathrm{L}1} & \mathbf{H}_{\mathrm{LL}} & \mathbf{H}_{\mathrm{LB}}\\ \mathbf{H}_{\mathrm{B}1} & \mathbf{H}_{\mathrm{BL}} & \mathbf{H}_{\mathrm{BB}}\end{bmatrix},\ \mathbf{J}=\begin{bmatrix}\mathbf{J}_{11} & \mathbf{J}_{1\mathrm{L}} & \mathbf{J}_{1\mathrm{B}}\\ \mathbf{J}_{\mathrm{L}1} & \mathbf{J}_{\mathrm{LL}} & \mathbf{J}_{\mathrm{LB}}\\ \mathbf{J}_{\mathrm{B}1} & \mathbf{J}_{\mathrm{BL}} & \mathbf{J}_{\mathrm{BB}}\end{bmatrix},$$

where $\mathbf{G}_{11}=\mathbb{D}_{12}+\mathbb{D}_{34}+\mathbb{D}_{32}\lambda_y^{-1}+\mathbb{D}_{14}\lambda_y$, $\mathbf{G}_{1\mathrm{L}}=\mathbb{D}_{1\mathrm{R}}+\mathbb{D}_{3\mathrm{R}}\lambda_y^{-1}$, $\mathbf{G}_{1\mathrm{B}}=\mathbf{0}$, $\mathbf{G}_{\mathrm{L}1}=\mathbb{D}_{\mathrm{L}2}+\mathbb{D}_{\mathrm{L}4}\lambda_y$, $\mathbf{G}_{\mathrm{LL}}=\mathbb{D}_{\mathrm{LR}}$, $\mathbf{G}_{\mathrm{LB}}=\mathbf{0}$, $\mathbf{G}_{\mathrm{B}1}=\mathbb{D}_{\mathrm{B}2}+\mathbb{D}_{\mathrm{T}4}+\mathbb{D}_{\mathrm{T}2}\lambda_y^{-1}+\mathbb{D}_{\mathrm{B}4}\lambda_y$, $\mathbf{G}_{\mathrm{BL}}=\mathbb{D}_{\mathrm{BR}}+\mathbb{D}_{\mathrm{TR}}\lambda_y^{-1}$, $\mathbf{G}_{\mathrm{BB}}=\mathbf{0}$, $\mathbf{H}_{11}=\mathbb{D}_{11}+\mathbb{D}_{22}+\mathbb{D}_{33}+\mathbb{D}_{44}+(\mathbb{D}_{31}+\mathbb{D}_{42})\lambda_y^{-1}+(\mathbb{D}_{13}+\mathbb{D}_{24})\lambda_y$, $\mathbf{H}_{1\mathrm{L}}=\mathbb{D}_{1\mathrm{L}}+\mathbb{D}_{2\mathrm{R}}+(\mathbb{D}_{3\mathrm{L}}+\mathbb{D}_{4\mathrm{R}})\lambda_y^{-1}$, $\mathbf{H}_{1\mathrm{B}}=\mathbb{D}_{1\mathrm{B}}+\mathbb{D}_{3\mathrm{T}}+\mathbb{D}_{3\mathrm{B}}\lambda_y^{-1}+\mathbb{D}_{1\mathrm{T}}\lambda_y$, $\mathbf{H}_{\mathrm{L}1}=\mathbb{D}_{\mathrm{L}1}+\mathbb{D}_{\mathrm{R}2}+\mathbb{D}_{\mathrm{L}3}\lambda_y^{-1}+\mathbb{D}_{\mathrm{R}4}\lambda_y$, $\mathbf{H}_{\mathrm{LL}}=\mathbb{D}_{\mathrm{LL}}+\mathbb{D}_{\mathrm{RR}}$, $\mathbf{H}_{\mathrm{LB}}=\mathbb{D}_{\mathrm{LB}}+\mathbb{D}_{\mathrm{LT}}\lambda_y$, $\mathbf{H}_{\mathrm{B}1}=\mathbb{D}_{\mathrm{B}1}+\mathbb{D}_{\mathrm{T}3}+\mathbb{D}_{\mathrm{T}1}\lambda_y^{-1}+\mathbb{D}_{\mathrm{B}3}\lambda_y$, $\mathbf{H}_{\mathrm{BL}}=\mathbb{D}_{\mathrm{BL}}+\mathbb{D}_{\mathrm{TL}}\lambda_y^{-1}$, $\mathbf{H}_{\mathrm{BB}}=\mathbb{D}_{\mathrm{BB}}+\mathbb{D}_{\mathrm{TT}}+\mathbb{D}_{\mathrm{TB}}\lambda_y^{-1}+\mathbb{D}_{\mathrm{BT}}\lambda_y$, $\mathbf{J}_{11}=\mathbb{D}_{21}+\mathbb{D}_{43}+\mathbb{D}_{41}\lambda_y^{-1}+\mathbb{D}_{23}\lambda_y$, $\mathbf{J}_{1\mathrm{L}}=\mathbb{D}_{2\mathrm{L}}+\mathbb{D}_{4\mathrm{L}}\lambda_y^{-1}$, $\mathbf{J}_{1\mathrm{B}}=\mathbb{D}_{2\mathrm{B}}+\mathbb{D}_{4\mathrm{T}}+\mathbb{D}_{4\mathrm{B}}\lambda_y^{-1}+\mathbb{D}_{2\mathrm{T}}\lambda_y$, $\mathbf{J}_{\mathrm{L}1}=\mathbb{D}_{\mathrm{R}1}+\mathbb{D}_{\mathrm{R}3}\lambda_y$, $\mathbf{J}_{\mathrm{LL}}=\mathbb{D}_{\mathrm{RL}}$, $\mathbf{J}_{\mathrm{LB}}=\mathbb{D}_{\mathrm{RB}}+\mathbb{D}_{\mathrm{RT}}\lambda_y$, $\mathbf{J}_{\mathrm{B}1}=\mathbf{0}$, $\mathbf{J}_{\mathrm{BL}}=\mathbf{0}$, $\mathbf{J}_{\mathrm{BB}}=\mathbf{0}$.

References

[1] R. S. Langley, The response of two-dimensional periodic structures to point harmonic forcing, Journal of Sound and Vibration 197 (1996) 447–469.

[2] A. C. Eringen, D. G. B. Edelen, On nonlocal elasticity, International Journal of Engineering Science 10 (1972) 233–248.

[3] M. Chen, S. Xu, L. Yuan, C. Miao, J. Lu, H. Ma, G. Gao, P. Wang, Influence of stress state on dynamic behaviors of concrete under true triaxial confinements, International Journal of Mechanical Sciences (2023) 108399.

[4] Z. Fu, W. Chen, P. Wen, C. Zhang, Singular boundary method for wave propagation analysis in periodic structures, Journal of Sound and Vibration 425 (2018) 170–188.

[5] R. Vescovini, N. Fantuzzi, Free vibrations of conical shells via ritz method, International Journal of Mechanical Sciences (2022) 107925.

[6] P. Fernando, D. Mohotti, A. Remennikov, P. Hazell, H. Wang, A. Amin, Experimental, numerical and analytical study on the shock wave propagation through impedance-graded multi-metallic systems, International Journal of Mechanical Sciences 178 (2020) 105621.

[7] S. Ravindran, B. Koohbor, P. Malchow, A. Kidane, Experimental characterization of compaction wave propagation in cellular polymers, International Journal of Solids and Structures 139 (2018) 270–282.

[8] Y. Wang, Z. Zheng, F. Zeng, M. Fu, Geometrical and microstructural size effects in progressive forming using wires, International Journal of Mechanical Sciences 251 (2023) 108332.

[9] Z. Zheng, M. Zhan, M. Fu, Microstructural and geometrical size effects on the fatigue of metallic materials, International Journal of Mechanical Sciences 218 (2022) 107058.

[10] B. Zhang, H. Li, L. Kong, J. Wang, H. Shen, Strain gradient differential quadrature beam finite elements, Computers & Structures 218 (2019) 170–189.

[11] J. Hamilton, W. Wolfer, Theories of surface elasticity for nanoscale objects, Surface Science 603 (9) (2009) 1284–1291.

[12] V. A. Eremeyev, G. Rosi, S. Naili, Transverse surface waves on a cylindrical surface with coating, International Journal of Engineering Science 147 (2020) 103188.

[13] S. El-Sapa, Effect of magnetic field on a microstretch fluid drop embedded in an unbounded another microstretch fluid, European Journal of Mechanics-B/Fluids 85 (2021) 169–180.

[14] Y. Chen, J. D. Lee, Determining material constants in micromorphic theory through phonon dispersion relations, International Journal of Engineering Science 41 (8) (2003) 871–886.

[15] X. Zeng, Y. Chen, J. D. Lee, Determining material constants in nonlocal micromorphic theory through phonon dispersion relations, International journal of engineering science 44 (18-19) (2006) 1334–1345.

[16] T. Aksencer, M. Aydogdu, Levy type solution method for vibration and buckling of nanoplates using nonlocal elasticity theory, Physica E: Low-dimensional Systems and Nanostructures 43 (4) (2011) 954–959.

[17] M. R. Barati, Vibration analysis of porous fg nanoshells with even and uneven porosity distributions using nonlocal strain gradient elasticity, Acta Mechanica 229 (3) (2018) 1183–1196.

[18] R. E. Miller, V. B. Shenoy, Size-dependent elastic properties of nano-sized structural elements, Nanotechnology 11 (3) (2000) 139.

[19] M. Lazar, G. A. Maugin, E. C. Aifantis, Dislocation in second strain gradient elasticity, International Journal of Solids and Structures (2006) 1787–1817.

[20] M. Arefi, M. Kiani, T. Rabczuk, Application of nonlocal strain gradient theory to size dependent bending analysis of a sandwich porous nanoplate integrated with piezomagnetic face-sheets, Composites Part B: Engineering 168 (2019) 320–333.

[21] A. Eringen, Simple microfluids, International Journal of Engineering Science 2 (1964) 205–217.

[22] A. Eringen, Linear theory of micropolar elasticity, Journal of Applied Mathematics and Mechanics 15 (1966) 909–923.

[23] E. Kroner, Elasticity theory of materials with long range cohesive forces, International Journal of Solids and Structures 3 (1967) 731–742.

[24] A. Muc, Non-local approach to free vibrations and buckling problems for cylindrical nano-structures, Composite Structures 250 (2020) 112541.

[25] M. E. Gurtin, A. I. Murdoch, A continuum theory of elastic material surfaces, Archive for rational mechanics and analysis 57 (4) (1975) 291–323.

[26] L. Li, R. Lin, T. Y. Ng, Contribution of nonlocality to surface elasticity, International Journal of Engineering Science 152 (2020) 103311.

[27] M. M. S. Fakhrabadi, Prediction of small-scale effects on nonlinear dynamic behaviors of carbon nanotube-based nano-resonators using consistent couple stress theory, Composites Part B: Engineering 88 (2016) 26–35.

[28] H. Shodja, A. Goodarzi, M. Delfani, H. Haftbaradaran, Scattering of an anti-plane shear wave by an embedded cylindrical micro-/nano-fiber within couple stress theory with micro inertia, International Journal of Solids and Structures 58 (2015) 73–90.

[29] S. J. Behrouz, O. Rahmani, S. A. Hosseini, On nonlinear forced vibration of nano cantilever-based biosensor via couple stress theory, Mechanical Systems and Signal Processing 128 (2019) 19–36.

[30] R. D. Mindlin, Micro-structure in linear elasticity, Archive for Rational Mechanics and Analysis 16 (1964) 51–78.

[31] B. Karami, M. Janghorban, A. Tounsi, Variational approach for wave dispersion in anisotropic doubly-curved nanoshells based on a new nonlocal strain gradient higher order shell theory, Thin-Walled Structures 129 (2018) 251–264.

[32] R. D. Mindlin, Second gradient of strain and surface tension in linear elasticity, International Journal of Solids and Structures (1965) 147–438.

[33] N. M. Cordero, S. Forest, E. P. Busso, Second strain gradient elasticity of nano-objects, Journal of the Mechanics and Physics of Solids 97 (2016) 92–124.

[34] A. M. Dehrouyeh-Semnani, M. Nikkhah-Bahrami, The influence of size-dependent shear deformation on mechanical behavior of microstructures-dependent beam based on modified couple stress theory, Composite Structures 123 (2015) 325–336.

[35] X. Yu, A. Maalla, Z. Moradi, Electroelastic high-order computational continuum strategy for critical voltage and frequency of piezoelectric nems via modified multi-physical couple stress theory, Mechanical Systems and Signal Processing 165 (2022) 108373.

[36] M. Lazar, G. A. Maugin, Nonsingular stress and strain fields of dislocations and disclinations in first strain gradient elasticity, International journal of engineering science 43 (13-14) (2005) 1157–1184.

[37] M. Lazar, G. A. Maugin, E. C. Aifantis, Dislocations in second strain gradient elasticity, International Journal of Solids and Structures 43 (6) (2006) 1787–1817.

[38] A. C. Eringen, Linear theory of micropolar elasticity, Journal of Mathematics and Mechanics (1966) 909–923.

[39] E. Kröner, Elasticity theory of materials with long range cohesive forces, International Journal of Solids and Structures 3 (5) (1967) 731–742.

[40] M. E. Gurtin, A. I. Murdoch, Surface stress in solids, International Journal of Solids and Structures 14 (6) (1978) 431–440.

[41] B. Yang, C. Droz, A. Zine, M. Ichchou, Dynamic analysis of second strain gradient elasticity through a wave finite element approach, Composite Structures 263 (2021). doi:https://doi.org/10.1016/j.compstruct.2020.113425.

[42] G. Bruno, M. Kachanov, Microstructure–property connections for porous ceramics: the possibilities offered by micromechanics, Journal of the American Ceramic Society 99 (12) (2016) 3829–3852.

[43] M. Bacciocchi, N. Fantuzzi, R. Luciano, A. M. Tarantino, Linear eigenvalue analysis of laminated thin plates including the strain gradient effect by means of conforming and nonconforming rectangular finite elements, Computers & Structures 257 (2021) 106676.

[44] M. Bacciocchi, N. Fantuzzi, A. Ferreira, Conforming and nonconforming laminated finite element kirchhoff nanoplates in bending using strain gradient theory, Computers & Structures 239 (2020) 106322.

[45] M. Bacciocchi, N. Fantuzzi, R. Luciano, A. M. Tarantino, Finite element solution of vibrations and buckling of laminated thin plates in hygro-thermal environment based on strain gradient theory, Mechanics of Advanced Materials and Structures (2022) 1–14.

[46] G. Tocci Monaco, N. Fantuzzi, F. Fabbrocino, R. Luciano, Semi-analytical static analysis of nonlocal strain gradient laminated composite nanoplates in hygrothermal environment, Journal of the Brazilian Society of Mechanical Sciences and Engineering 43 (5) (2021) 1–20.

[47] G. Fu, S. Zhou, L. Qi, On the strain gradient elasticity theory for isotropic materials, International Journal of Engineering Science 154 (2020) 103348.

[48] M. Tuna, L. Leonetti, P. Trovalusci, M. Kirca, 'explicit'and 'implicit'non-local continuous descriptions for a plate with circular inclusion in tension, Meccanica 55 (4) (2020) 927–944.

[49] M. Tuna, P. Trovalusci, Scale dependent continuum approaches for discontinuous assemblies:'explicit'and 'implicit'non-local models, Mechanics Research Communications 103 (2020) 103461.

[50] N. Fantuzzi, P. Trovalusci, R. Luciano, Material symmetries in homogenized hexagonal-shaped composites as cosserat continua, Symmetry 12 (3) (2020) 441.

[51] S. A. Faghidian, K. K. Żur, J. N. Reddy, A. J. M. Ferreira, On the wave dispersion in functionally graded porous timoshenko-ehrenfest nanobeams based on the higher-order nonlocal gradient elasticity, Composite Structures 279 (2022) 114819.

[52] S. A. Faghidian, K. K. Żur, E. Pan, Stationary variational principle of mixture unified gradient elasticity, International Journal of Engineering Science 182 (2023) 103786.

[53] S. A. Faghidian, K. K. Żur, J. N. Reddy, A mixed variational framework for higher-order unified gradient elasticity, International Journal of Engineering Science 170 (2022) 103603.

[54] J. M. Mencik, M. N. Ichchou, Wave finite elements in guided elastodynamics with internal fluid, International Journal of Solids and Structures 44 (2007) 2148–2167.

[55] C. Droz, J. P. Lainé, M. N. Ichchou, G. Inquiété, A reduced formulation for the free-wave propagation analysis in composite structures, Composite Structures 113 (2014) 134–144.

[56] F. Errico, M. Ichchou, S. De Rosa, F. Franco, O. Bareille, Investigations about periodic design for broadband increased sound transmission loss of sandwich panels using 3d-printed models, Mechanical Systems and Signal Processing 136 (2020) 106432.

[57] R. Singh, C. Droz, M. Ichchou, F. Franco, O. Bareille, S. De Rosa, Stochastic wave finite element quadratic formulation for periodic media: 1d and 2d, Mechanical Systems and Signal Processing 136 (2020) 106431.

[58] D. Mead, A general theory of harmonic wave propagation in linear periodic systems with multiple coupling, Journal of Sound and Vibration 27 (1973) 235–260.

[59] M. Ichchou, F. Bouchoucha, M. B. Souf, O. Dessombz, M. Haddar, Stochastic wave finite element for random periodic media through first-order perturbation, Computer Methods in Applied Mechanics and Engineering 200 (41-44) (2011) 2805–2813.

[60] D. Duhamel, B. R. Mace, M. Brennan, Finite element analysis of the vibrations of waveguides and periodic structures, Journal of Sound and Vibration 294 (2006) 205–220.

[61] Y. Xiao, J. Wen, D. Yu, X. Wen, Flexural wave propagation in beams with periodically attached vibration absorbers: Band-gap behavior and band formation mechanisms, Journal of Sound and Vibration 332 (4) (2013) 867–893.

[62] Y. Wei, G. Hu, Wave characteristics of extremal elastic materials, Extreme Mechanics Letters 55 (2022) 101789.

[63] K. Zhang, P. Zhao, C. Zhao, F. Hong, Z. Deng, Study on the mechanism of band gap and directional wave propagation of the auxetic chiral lattices, Composite Structures 238 (2020) 111952.

[64] H. Nguyen, R. Tsai, Numerical wave propagation aided by deep learning, Journal of Computational Physics 475 (2023) 111828.

[65] H. M. Shodja, F. Ahmadpoor, T. A., Calculation of the additional constants for fcc materials in second strain gradient elasticity: behavior of a nano-size bernoulli-euler beam with surface effects, Applied Mechanics 72 (2) (2010) 021008.

[66] J. Q. Zhao, P. Zeng, B. Pan, Improved hermite finite element smoothing method for full-field strain measurement over arbitrary region of interest in digital image correlation, Optics and Lasers in Engineering 50 (2012) 1662–1671.

[67] I. Bennamia, A. Badereddine, T. Zebbiche, Measurement of vibrations of composite wings using high-order finite element beam, Journal of Measurements in Engineering 6 (2018) 143–154.

[68] S. Khakalo, J. Niiranen, Form ii of mindlin's second strain gradient theory of elasticity with a simplification: For materials and structures from nano- to macro-scales, European Journal of Mechanics / A Solids 71 (2018) 292–319.

[69] V. Balobanov, J. Niiranen, Locking-free variational formulations and isogeometric analysis for the timoshenko beam models of strain gradient and classical elasticity, Computer Methods in Applied Mechanics and Engineering 339 (2018) 137–159.

[70] W.-J. Beyn, An integral method for solving nonlinear eigenvalue problems, Linear Algebra and its Applications 436 (10) (2012) 3839–3863.

[71] P. Puri, V. Yang, Thermo-mechanical behavior of nano aluminum particles with oxide layers during melting, Journal of nanoparticle research 12 (2010) 2989–3002.

[72] L. Li, Y. Hu, Post-buckling analysis of functionally graded nanobeams incorporating nonlocal stress and microstructure-dependent strain gradient effects, International Journal of Mechanical Sciences 120 (2017) 159–170.

[73] K. Graff, Wave Motion in Elastic Solids, Oxford University Press, London, 1991, Ch. Longitudinal waves in the rods, pp. 75–130.

[74] V. Cotoni, R. Langley, P. Shorter, A statistical energy analysis subsystem formulation using finite element and periodic structure theory, Journal of Sound and Vibration 318 (2008) 1077–1108.